MOX-Report No. 54/2017

Isogeometric Analysis of a Phase Field Model for Darcy Flows with Discontinuous Data

Dede', L; Quarteroni, A.

MOX, Dipartimento di Matematica
Politecnico di Milano, Via Bonardi 9 - 20133 Milano (Italy)

mox-dmat@polimi.it http://mox.polimi.it

Isogeometric Analysis of a Phase Field Model for Darcy Flows with Discontinuous Data

Luca Dedè[*,†], Alfio Quarteroni[♯]

[†] MOX – Modeling and Scientific Computing
Mathematics Department "F. Brioschi"
Politecnico di Milano
P.zza Leonardo da Vinci 32, 20133 Milano, Italy

[♯] CMCS – Chair of Modeling and Scientific Computing
MATH – Section of Mathematics
EPFL – Ećole Polytechnique Fédérale de Lausanne
Station 8, Lausanne, CH–1015, Switzerland

October 20, 2017

Abstract

We consider a phase field model for Darcy flows with discontinuous data in porous media; specifically, we adopt the Hele–Shaw–Cahn–Hillard equations of [Lee, Lowengrub, Goodman, Physics of Fluids, 2002] to model flows in the Hele–Shaw cell through a phase field formulation which incorporates discontinuities of physical data, namely density and viscosity, across interfaces. For the spatial approximation of the problem, we use NURBS–based Isogeometric Analysis in the framework of the Galerkin method, a computational framework which is particularly advantageous for the solution of high order Partial Differential Equations and phase field problems which exhibit sharp but smooth interfaces. In this paper, we verify through numerical tests the sharp interface limit of the phase field model which in fact leads to an internal discontinuity interface problem; finally, we show the efficiency of Isogeometric Analysis for the numerical approximation of the model by solving a benchmark problem, the so–called "rising bubble" problem.

Keywords. Darcy flows; Phase field; Hele–Shaw cell; Cahn–Hilliard equation; Sharp interface limit; Isogeometric Analysis.
MR 2000 Subject classification. 65L60; 74S05; 80A22.

[*]Corresponding author. E-mail: luca.dede@polimi.it, Phone: +32 02 23991 4642, Fax: +32 02 23991 4615.

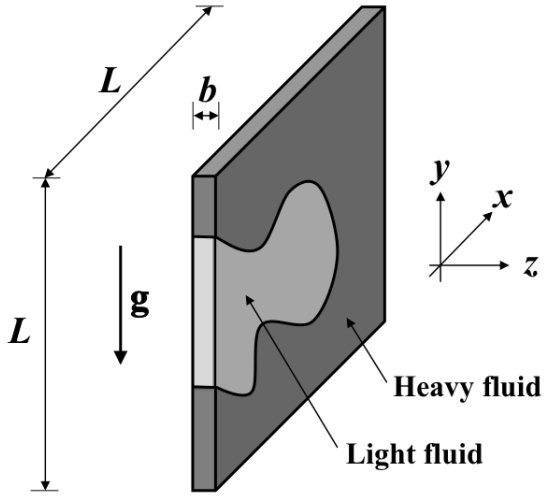

Figure 1: Hele–Shaw vertical cell containing light and heavy fluids under the effect of gravity.

1 Introduction

The Hele–Shaw model (flow) [7] describes the laminar motion of a (Newtonian) viscous fluid in an Hele–Shaw cell – also known as the Hele–Shaw analog or viscous flow analog – an experimental device composed by two parallel plates of size L kept at the distance b from each other, with $b \ll L$ (see Fig. 1). The vertical, horizontal or angled Hele–Shaw cells can be considered to possibly account for gravity effect. The device was firstly proposed and used by Hele–Shaw [33] to experimentally investigate the viscous (potential) flows around bodies; later, vertical Hele–Shaw cells have been extensively used to study groundwater flows, oil production, drainage, etc. A wide literature is available on the topic, see e.g. [7, 43, 49, 56]. Indeed, the importance of the Hele–Shaw model lays in the fact that the potential flow occurring in the Hele–Shaw cell corresponds to a Darcy flow in a porous media ([7]) with permeability equivalent to $\frac{b^2}{12}$ [49]. We observe that, even if the Hele–Shaw flow occurs only for two–dimensional laminar flows, it represents a valid simplified model with respect to the full Navier–Stokes equations to study the effect of flows in porous media provided that the three–dimensional effects are negligible; moreover, it provides a framework for experimental comparisons: as reported in [7] and the references herein indicated, the Hele–Shaw cell is suitable for flows with Reynolds numbers smaller than 500–1′000, these being defined by means of the distance between the plates b.

The Cahn–Hilliard equation is a time dependent, mass conservative phase field model which describes the segregation of the phases from a mixed configuration to a fully separated one, with the pure phases separated by smooth, but sharp interfaces [12, 13, 25]. The Cahn–Hilliard equation is a nonlinear, parabolic PDE with fourth–order spatial derivatives, which during the phase transition exhibits a fast and intermittent dynamics. It has been originally introduced by Cahn [12] to describe the separation of binary alloys systems in metallurgy and it later extensively studied both from a theoretical and numerical point of view, see e.g.

[5, 10, 20, 28, 29, 32, 45, 55].

The ideal combination of the Hele–Shaw model with the Cahn–Hilliard phase field model yields the so–called Hele–Shaw–Cahn–Hilliard equations. These represent indeed a phase field model for Hele–Shaw flows with physical data varying through the smooth but sharp interfaces; the physical data depend of the phase field variable whose distribution in the computational domain depend on the phase transition according to a generalized Cahn–Hilliard equation. In the limit of interface thickness tending to zero [45], these physical data are in fact discontinuous across the interface. The model has been developed in [39] as a special case of the Navier–Stokes–Cahn–Hilliard model for immiscible fluids proposed in [42] of which it represents a simplified version under the hypothesis of Hele–Shaw flow (the inertial forces are negligible with respect to the viscous ones). In particular, the model is only two–dimensional and valid for isothermal laminar flows among the plates of the Hele–Shaw cell provided that there are no variation of the phase variable through the thickness among the plates. Nevertheless, the phase field model (see also [16, 27, 37]) has the clear advantage of embedding into the formulation modifications in the shape of the interface and its evolution in time, as well as to naturally allow topological changes without resorting to interface capturing or tracking methods like the volume of fluid or level set methods [31, 34, 44, 50]. Moreover, the asymptotic, sharp interface limit of the phase field model [11] yields the Darcy flow problem with internally discontinuous data across the interface [42].

The analysis of Hele–Shaw–Cahn–Hilliard equations and related models is particularly challenging. For example, the well–posedness of Navier–Stokes–Cahn–Hilliard model has been studied in [53] and its long time behavior described in [52]. The convergence of weak solutions of the Cahn–Hilliard—Brinkman model to the Hele–Shaw–Cahn–Hilliard equations has been proved in [9] and a non–local solution of the previous result determined in [47]. The global, sharp interface limit of these equations has been recently studied in [21]. More recently, an alternative Hele–Shaw–Cahn–Hilliard model has been derived in [18] (starting from [2]) and therein analyzed using a volume–averaged definition of the velocity field instead of the mass–averaged one of [39]; see also [1] for the application of the model to tumor modeling. In this paper, however we refer to the original formulation of the Hele–Shaw–Cahn–Hilliard equations proposed in [39].

The phase field model based on the Hele–Shaw–Cahn–Hilliard equations inherits similar mathematical features of the Cahn–Hilliard equations. It is a nonlinear system of Partial Differential Equations (PDEs) in parabolic–elliptic formulation in the phase field and pressure variables, respectively, which involves high order spatial derivatives (up to four) for the phase field variable, whose solution may exhibit fast and intermittent dynamics. For these reasons, the numerical approximation of this problem is particularly challenging as an accurate and efficient numerical method should be able to cope with all these features. Spatial approximations using the Finite Element method with the standard Lagrange polynomial basis have been widely adopted for phase field models [22, 23, 24, 54] even if the fourth order derivatives involved in the problem require to resort to mixed formulations. In this paper, we propose instead NURBS–based Isogeometric Analysis in the framework of the Galerkin method [15, 35] for spatially approximating such high order PDEs. Isogeometric Analysis is a discretization method based on the isogeometric paradigm, for which the

same basis functions are used first for the representation of the domain and then for the approximation of the solution of the PDEs. Besides of the geometric advantages related to this choice, the employment of high order continuous NURBS or B–splines basis functions to build the trial and test function subspaces allows solving the phase field model in the framework of the standard Galerkin formulation [51]. In particular, globally C^1–continuous B–splines basis functions of degree $p = 2$ allow the construction of trial and test function subspaces which are H^2–conformal; moreover, these basis functions facilitate the introduction of periodic boundary conditions. These features of B–splines and NURBS basis functions have been extensively exploited for solving phase field model together with their accuracy in representing sharp but smooth interfaces, see e.g. [6, 17, 28, 30, 41]. In this paper, we use Isogeometric Analysis for solving the Hele–Shaw–Cahn–Hilliard equations for fluids in porous media endowed with discontinuous data, in particular the density; in this respect, we efficiently solve by means of our formulation the "rising bubble" benchmark problem [36]. In addition, we use the proposed method to verify the sharp interface limit of the Hele–Shaw–Cahn–Hilliard equations and we show that this phase field model can be efficiently used to represent an interface discontinuity problem involving the Poisson equation [19] without resorting to interface tracking or interface capturing techniques.

This paper is organized as follows. In Sec. 2 we recall the Hele–Shaw and Cahn–Hilliard equations and then the phase field model described by the Hele–Shaw–Chan–Hilliard equations; we also discuss their sharp interface limit. In Sec. 3 we present the numerical discretization of the problem based on Isogeometric Analysis. In Sec. 4 we numerically verify the sharp interface limit of the model and we solve the benchmark problem of the "rising bubble". Conclusions follow.

2 Phase Field Model

In this section, we recall the basic notions of the Hele–Shaw and Cahn–Hilliard models. We provide the formulation of the Hele–Shaw–Cahn–Hilliard equations based on [39, 40], their dimensionless form, the sharp interface limit, and the weak formulation of the problem.

2.1 The Hele–Shaw and Darcy flows

In this work, we are principally interested in flows under the effect of the gravity and therefore, we consider the vertical Hele–Shaw flow for the vertical analog [7]. Still referring to Fig. 1, we assume that the Hele–Shaw cell lays in the plane x–y with center in z = 0 such that $\mathrm{z} \in \left(-\frac{b}{2}, \frac{b}{2}\right)$; we introduce the velocity variable $\mathbf{V} := u\,\hat{\mathbf{x}} + v\,\hat{\mathbf{y}} + w\,\hat{\mathbf{z}}$, the pressure variable P, the constant density ρ, the constant dynamic viscosity η and the gravity $\mathbf{g} = g\,\hat{\mathbf{g}}$, where the unit vector $\hat{\mathbf{g}} := g_{\mathrm{x}}\,\hat{\mathbf{x}} + g_{\mathrm{y}}\,\hat{\mathbf{y}}$ indicates the direction of the gravity and g the modulus. To derive the Hele–Shaw flow starting from the Navier–Stokes equations, we assume that $\mathbf{V} = \mathbf{0}$ at the walls of the plates, $w = 0$ and the velocity gradients in the x and y directions

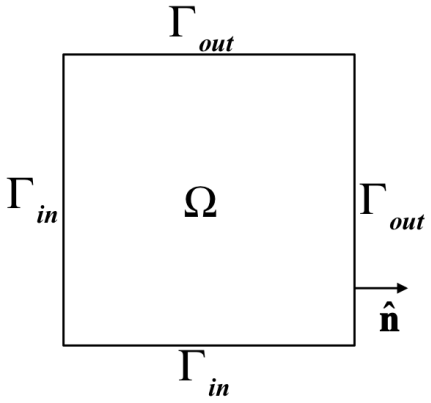

Figure 2: Computational domain Ω, boundaries Γ_{in} and Γ_{out} for the imposition of pairs of periodic boundary conditions and unit vector $\hat{\mathbf{n}}$ normal to $\partial\Omega = \Gamma_{in} \cup \Gamma_{out}$.

are negligible with respect to those in the z direction. The Hele–Shaw flow velocity reads [7]:

$$\mathbf{V} = -\frac{1}{2\eta}\left(\frac{b^2}{4} - z^2\right)\nabla\left(P - \rho\, g\, \varphi_P\right), \tag{2.1}$$

with the gravitational potential φ_p:

$$\varphi_p := \hat{\mathbf{g}} \cdot \left((\mathrm{x} - \mathrm{x}_0)\,\hat{\mathbf{x}} + (\mathrm{y} - \mathrm{y}_0)\,\hat{\mathbf{y}}\right), \tag{2.2}$$

defined in terms of a reference coordinate $\mathbf{x}_0 := (\mathrm{x}_0, \mathrm{y}_0)$ and $\dfrac{\partial}{\partial z}\left(P - \rho\, g\, \varphi_P\right) = 0$; in this manner, we have that $\mathbf{V} = \mathbf{V}(\mathrm{x}, \mathrm{y}, \mathrm{z})$, while $P = P(\mathrm{x}, \mathrm{y})$. By introducing the specific discharge $\mathbf{Q}$ in the interspace between the two plates, i.e. the averaged velocity through the thickness $\mathbf{Q} := \dfrac{1}{b}\displaystyle\int_{-b/2}^{b/2} \mathbf{V}\, dz$, we have:

$$\mathbf{Q} = -\frac{b^2}{12\,\eta}\nabla\left(P - \rho\, g\, \varphi_P\right), \tag{2.3}$$

with $\mathbf{Q} = \mathbf{Q}(\mathrm{x}, \mathrm{y})$ as for the pressure P. It is straightforward to deduce the analogy of the Hele–Shaw flow with the two–dimensional Darcy law, since mass conservation leads to the requirement that $\nabla \cdot \mathbf{Q} = 0$ in the computational domain, with $\dfrac{b^2}{12}$ representing the permeability of the porous medium.

2.2 The Cahn–Hilliard equation

In order to recall the isothermal Cahn–Hilliard equation for a binary fluid with constant density ρ, let us denote with c the dimensionless concentration of one of the phase variables defined in a computational domain $\Omega \subset \mathbb{R}^2$ as the one represented in Fig. 2. We specifically

consider for example the case of periodic boundary conditions (see e.g. [28, 41]), even if other cases can be considered as well [1]. Albeit flow problems in the Hele–Shaw vertical cell – as that depicted in Fig. 1 – appear, at first glance, far from carrying periodic boundary conditions, we will see later that these conditions can instead be conveniently applied under certain circumstances. With this aim, let us introduce the notation Γ_{in} and Γ_{out} to indicate the subsets of the boundary $\partial\Omega$ on which the pairs of periodic boundary conditions will be imposed, where $\Gamma_{in} \cup \Gamma_{out} = \partial\Omega$ and $\Gamma_{in} \cap \Gamma_{out} = \emptyset$ a.e.; the vector $\hat{\mathbf{n}}$ represents the outward directed unit vector normal to $\partial\Omega$ (Γ_{in} or Γ_{out}).

In addition, we introduce a total free energy, say $E_{CH}(c)$. For the problem under consideration, in which c is the unique dependent variable and the density ρ constant, we assume:

$$E_{CH}(c) := \int_{\Omega} \rho\, f(c)\, d\Omega, \tag{2.4}$$

where the total free energy function (Helmholtz potential) $f(c) = \widehat{f}(c, \nabla c)$ is defined as:

$$f(c) := \widehat{f}(c, \nabla c) = \sigma\, f_0(c) + \frac{1}{2}\,\lambda\, \nabla c \cdot \nabla c, \tag{2.5}$$

with $f_0(c)$ the bulk energy density function, and σ and λ suitable positive, dimensional parameters. We remark that the thickness of the interfaces among the pure phases is proportional to $\sqrt{\dfrac{\lambda}{\sigma}}$. Following [42], we define the chemical potential $\mu_{CH}(c)$ in the case of the isothermal Cahn–Hilliard equation with constant density as:

$$\mu_{CH} := \frac{\partial \widehat{f}}{\partial c}(c) - \frac{1}{\rho}\nabla \cdot \left(\rho \frac{\partial \widehat{f}}{\partial \nabla c}(c) \right), \tag{2.6}$$

which assumes the explicit form $\mu_{CH}(c) = \sigma\, \dfrac{df_0}{dc}(c) - \lambda \Delta c$.

We remark that the choice of the bulk energy density function $f_0(c)$ determines the separation of the phases typical in immiscible fluids, provided that it is in general non convex and in the form of a double–well function in the variable c, with the pure phases in c_1 and c_2; in particular, we choose the following quartic form for $f_0(c)$:

$$f_0(c) := c^2\, (1 - c)^2\,, \tag{2.7}$$

which is polynomial, differentiable in c and with the pure phases in $c_1 = 1$ and $c_2 = 0$ [2].

[1] We remark that pairs of compatible boundary conditions need to be specified on each subset of the boundary $\partial\Omega$ due to the fourth–order spatial operator characterizing the Cahn–Hilliard equation.

[2] A typical choice for $f_0(c)$ is represented by the logarithm function with singular values (see e.g. [13]); for an alternative choice see e.g. [17].

Finally, the isothermal Cahn–Hilliard equation with constant density and periodic boundary conditions reads:

$$\begin{aligned}
&\frac{\partial c}{\partial t} = \nabla \cdot (D_0 \nabla \mu_{CH}(c)) && \text{in } \Omega,\ \forall t \in (0,T),\\
&c|_{\Gamma_{in}} = c|_{\Gamma_{out}} && \forall t \in (0,T),\\
&(\nabla c \cdot \hat{\mathbf{n}})\,|_{\Gamma_{in}} = -\,(\nabla c \cdot \hat{\mathbf{n}})\,|_{\Gamma_{out}} && \forall t \in (0,T),\\
&c = c_0 && \text{in } \Omega,\ t = 0.
\end{aligned} \tag{2.8}$$

where $D_0 > 0$ is the mobility which we assume constant (with the dimension of a diffusivity); $c|_{\Gamma_{in}} = c|_{\Gamma_{out}}$ and $(\nabla c \cdot \hat{\mathbf{n}})\,|_{\Gamma_{in}} = -\,(\nabla c \cdot \hat{\mathbf{n}})\,|_{\Gamma_{out}}$ are abridged notations to indicate periodic boundary conditions. For example, if $\Omega = (0, L_0)^2$ with $\Gamma_{in} = \big\{(\mathrm{x},\mathrm{y}) \in \mathbb{R}^2 \ :\ \mathrm{x} = 0,\ \mathrm{y} \in (0, L_0)\big\}$ and $\Gamma_{out} = \big\{(\mathrm{x},\mathrm{y}) \in \mathbb{R}^2 \ :\ \mathrm{x} = L_0,\ \mathrm{y} \in (0, L_0)\big\}$, these conditions are being understood as $c(0,\mathrm{y}) = c(L_0,\mathrm{y})$ and, $\dfrac{\partial c}{\partial \mathrm{x}}(0,\mathrm{y}) = \dfrac{\partial c}{\partial \mathrm{x}}(L_0,\mathrm{y})$ for $\mathrm{y} \in (0, L_0)$.

We observe that the total free energy $E_{CH}(c)$ associated to the Cahn–Hilliard equation represents a Liapunov functional, i.e. $\dfrac{dE_{CH}}{dt}(c) \le 0$ for all $t \in [0,T)$, and the system is mass conservative in the sense that $\dfrac{dM}{dt}(c) = 0$, with $M(c) := \displaystyle\int_\Omega \rho\, c\, d\Omega$.

2.3 The Hele–Shaw–Cahn–Hilliard equations

In this section, we briefly recall the Hele–Shaw–Cahn–Hilliard equations in the pressure and phase field variables and we highlight their properties. For their detailed derivation and thermodynamical aspects we refer the interested reader to [39, 40] and also [42].

We start by assuming that the pure phases of the phase variable c are $c_1 = 1$ and $c_2 = 0$. We define the phase dependent density $\rho(c)$ for a mixture as:

$$\rho(c) := \frac{1}{\dfrac{1}{\rho_1}\, c + \dfrac{1}{\rho_2}\,(1-c)}, \tag{2.9}$$

and the phase dependent dynamic viscosity $\eta(c)$ as:

$$\eta(c) := \eta_1\, c + \eta_2\,(1-c), \tag{2.10}$$

for some constant densities ρ_i and dynamic viscosities η_i for $i = 1, 2$; we observe that when $c = c_i$, we have $\rho = \rho_i$ and $\eta = \eta_i$ for $i = 1, 2$. In addition, we introduce the following coefficient α, which possesses the dimension of an inverse density, as:

$$\alpha := \frac{1}{\rho_1} - \frac{1}{\rho_2} = -\,\frac{1}{(\rho(c))^2}\,\frac{d\rho}{dc}(c). \tag{2.11}$$

Also, in place of the pressure variable P introduced in Sec. 2.1, we consider an averaged pressure which filters the gravitational effect and it is particularly suitable for the imposition

of periodic boundary conditions. Specifically, we define:

$$p := P - p_{avg}, \tag{2.12}$$

where from Eq. (2.2) the average pressure $p_{avg} = p_{avg}(\mathbf{x})$ is:

$$p_{avg} := \rho_{avg}\, g\, \varphi_p, \tag{2.13}$$

with the average density:

$$\rho_{avg} := \frac{1}{|\Omega|} \int_\Omega \rho(c)\, d\Omega. \tag{2.14}$$

We introduce the surface tension vector $\mathbf{s}(c)$ which reads:

$$\mathbf{s}(c) := \lambda\, \nabla \cdot (\rho(c)\, \nabla c \otimes \nabla c)\,. \tag{2.15}$$

In this manner, the specific discharge $\mathbf{Q}$ introduced in Sec. 2.1 for the Hele–Shaw flow is modified in $\mathbf{q} = \mathbf{q}(p, c)$ to take into account for the dependency of the viscosity and density on c and the surface tension $\mathbf{s}(c)$:

$$\mathbf{q}(p, c) := -\frac{b^2}{12\, \eta(c)} \left(\nabla p + \mathbf{s}(c) + (\rho_{avg} - \rho(c))\; g\, \hat{\mathbf{g}}\right); \tag{2.16}$$

$\mathbf{q}(p, c)$ is also referred to as mass–averaged velocity. Furthermore, for the sake of simplicity, we define the flux $\theta(p, c, \dot{c})$, for which we highlight the explicit dependency on the time derivative on the phase variable c, as:

$$\theta\left(p, c, \frac{\partial c}{\partial t}\right) := \rho(c) \left(\frac{\partial c}{\partial t} + \mathbf{q}(p, c) \cdot \nabla c\right). \tag{2.17}$$

We introduce the total free energy $E(p, c)$ in a similar manner for the Cahn–Hilliard equation of Sec. 2.2 to include the potential energy associated to the gravitational effect, which reads:

$$E(p, c) := b \int_\Omega \rho(c)\; (f(c) - g\, \varphi_P)\; d\Omega, \tag{2.18}$$

with the free energy function $f(c)$ given in Eq. (2.5) and the gravitational potential φ_P in Eq. (2.2); we recall that Ω represents a two–dimensional computational domain and b is the distance between the plates of the Hele–Shaw cell. The chemical potential, let say $\mu(p, c)$, is defined in terms of the Gibbs energy $\mathcal{g}(p, c)$ for which we have the relation $\mathcal{g}(p, c) = f(c) + \dfrac{p + p_{avg}}{\rho(c)}$ in the isothermal case [42]. Specifically, we have that:

$$\mu(p, c) := \frac{\partial \widehat{f}}{\partial c}(c) - \frac{1}{\rho(c)} \nabla \cdot \left(\rho(c) \frac{\partial \widehat{f}}{\partial \nabla c}(c)\right) - \frac{1}{(\rho(c))^2}\, \frac{d\rho}{dc}(c)\; (p + p_{avg})\,, \tag{2.19}$$

with the explicit expression for the chemical potential $\mu(p, c)$ from Eqs. (2.5) and (2.11):

$$\mu(p, c) = \sigma\, \frac{df_0}{dc}(c) - \lambda\, \frac{1}{\rho(c)} \nabla \cdot (\rho(c) \nabla c) + \alpha\; (p + p_{avg})\,. \tag{2.20}$$

Finally, we provide the strong form of the Hele–Shaw–Cahn–Hilliard equations [39] endowed with periodic boundary conditions:

$$
\begin{aligned}
&\nabla \cdot \mathbf{q}(p,c) - \alpha\, \nabla \cdot (M_0 \nabla \mu(p,c)) = 0 && \text{in } \Omega,\ \forall t \in (0,T),\\
&\theta\left(p, c, \frac{\partial c}{\partial t}\right) - \nabla \cdot (M_0 \nabla \mu(p,c)) = 0 && \text{in } \Omega,\ \forall t \in (0,T),\\
&\int_\Omega p\, d\Omega = 0 && \forall t \in (0,T),\\
&p|_{\Gamma_{in}} = p|_{\Gamma_{out}} && \forall t \in (0,T),\\
&c|_{\Gamma_{in}} = c|_{\Gamma_{out}} && \forall t \in (0,T),\\
&(\nabla c \cdot \hat{\mathbf{n}})\,|_{\Gamma_{in}} = -\,(\nabla c \cdot \hat{\mathbf{n}})\,|_{\Gamma_{out}} && \forall t \in (0,T),\\
&c = c_0 && \text{in } \Omega,\ t = 0,
\end{aligned}
\tag{2.21}
$$

where the constant mobility $M_0 > 0$ assumes a role similar to the diffusivity D_0 introduced in Eq. (2.8) [3]. The first equation represents the modified Hele–Shaw equation, while the second is the modified Cahn–Hilliard equation which accounts for the pressure p. The system of PDEs (2.21) is parabolic with second–order spatial derivatives in the pressure variable p and fourth–order derivatives in the phase variable c; the time derivative appears explicitly only for the phase variable $\dfrac{\partial c}{\partial t}$, whereas the pressure variable p only depending implicitly on t through the phase transition. The requirement that the average pressure p is zero for all $t \in (0,T)$ is introduced to ensure that the pressure problem is well posed and it is compatible with the change of variables in Eq. (2.12). The Hele–Shaw–Cahn–Hilliard equation is referred as quasi–incompressible [2, 42] in the sense that, at the steady state, the model is incompressible except at the interfaces between the pure phases, provided that a full separation among them occurred; indeed, it is easy to see that in the pure phases, for which $\nabla c = \mathbf{0}$, we have $\nabla \cdot \mathbf{q}(p,c) = 0$ at the steady state; also, we observe that when the density is constant, i.e. $\rho(c) = \rho$ and $\alpha = 0$, the model is fully incompressible a.e. for all $t \in (0,T)$. Similarly to the Cahn–Hilliard equation, the total free energy $E(c)$ (2.18) is a Liapunov functional, i.e. $\dfrac{dE}{dt}(p,c) \leq 0$ for all $t \in (0,T)$; and the system is mass conservative since $\dfrac{dM}{dt}(c) = 0$ for all $t \in (0,T)$ for the periodic boundary conditions under consideration.

2.4 The dimensionless Hele–Shaw–Cahn–Hilliard equations

We rewrite the system of PDEs (2.21) in terms of dimensionless variables and parameters; we will denote with the superscript $*$ the dimensionless quantities. We start by introducing the scaling for the space and time variables $\mathbf{x}^* := \dfrac{\mathbf{x}}{L_0}$ and $t^* := \dfrac{t}{T_0}$ being L_0 and T_0 the

[3] The product $\left(\dfrac{M_0\,\sigma}{\rho_0}\right)$ dimensionally represents a diffusivity or kinematic viscosity (square length over time).

representative length and time scales, respectively. In addition we introduce the scalings p_0, ρ_0, η_0 and q_0 for the pressure, density, dynamic viscosity and velocity (specific discharge), respectively. In this manner, we set $p^* := \dfrac{p}{p_0}$ and $c^* := c$ since the phase variable is already dimensionless; moreover, we define $\eta^*(c^*) := \dfrac{\eta(c)}{\eta_0}$, $\rho^*(c^*) := \dfrac{\rho(c)}{\rho_0}$, the parameter $\alpha^* := \rho_0\,\alpha$ and $\mathbf{q}^*(p^*, c^*) := \dfrac{\mathbf{q}(p, c)}{q_0}$; we observe that $\eta_i^* := \dfrac{\eta_i}{\eta_0}$ and $\rho_i^* := \dfrac{\rho_i}{\rho_0}$ for $i = 1, 2$. In addition, we have that $\nabla^* \cdot = L_0\,\nabla \cdot$, $\dfrac{\partial \cdot}{\partial t^*} \cdot = T_0\,\dfrac{\partial \cdot}{\partial t}$, $f_0^*(c^*) = f_0(c)$, $\rho_{avg}^* = \dfrac{\rho_{avg}}{\rho_0}$, $\hat{\mathbf{g}}^* = \hat{\mathbf{g}}$ and $\varphi_p^* = \dfrac{\varphi_p}{L_0}$. By assuming that the representative quantities L_0, ρ_0 and η_0 are chosen a priori, we obtain through dimensional analysis that the representative time, pressure and velocity are $T_0 = \dfrac{L_0}{q_0}$, $p_0 = \rho_0\,g\,L_0$ and $q_0 = \dfrac{\rho_0\,g\,b^2}{\eta_0}$, respectively.

The system (2.21) depends on the three following dimensionless parameters:

$$\mathbb{C}a := \frac{1}{\sigma}\,\frac{\lambda}{L_0^2} \qquad \mathbb{M}a := \frac{g\,L_0}{\sigma} \qquad \mathbb{P}e := \frac{\rho_0\,q_0\,L_0}{M_0\,\sigma} = \mathbb{M}a\,\frac{\rho_0^2\,b^2}{M_0\,\eta_0}, \tag{2.22}$$

the first being the Cahn number, the second is an analogue of the Mach number and the latter the Péclet number, with definitions similar to those for the Navier–Stokes–Cahn–Hilliard equations in [42]. We remark that the Cahn number is related to the thickness of the interfaces between the pure phases, while the Mach number is related to the ratio between the pressure and chemical (surface tension) forces. We define the following dimensionless quantities:

$$\mathbf{s}^*(c^*) := \nabla^* \cdot (\rho^*(c^*)\,\nabla^* c^* \otimes \nabla^* c^*)\,, \tag{2.23}$$

$$\mathbf{q}^*(p^*, c^*) := -\frac{1}{12\,\eta^*(c^*)}\left(\nabla^* p^* + \frac{\mathbb{C}a}{\mathbb{M}a}\,\mathbf{s}^*(c^*) + \left(\rho_{avg}^* - \rho^*(c^*)\right)\hat{\mathbf{g}}\right), \tag{2.24}$$

$$\theta^*\left(p^*, c^*, \frac{\partial c^*}{\partial t^*}\right) := \rho^*(c^*)\left(\frac{\partial c^*}{\partial t^*} + \mathbf{q}^*(p^*, c^*)\cdot\nabla^* c^*\right), \tag{2.25}$$

$$\mu^*(p^*, c^*) := \frac{df_0^*}{dc}(c^*) - \mathbb{C}a\,\frac{1}{\rho^*(c^*)}\nabla^*\cdot(\rho^*(c^*)\nabla^* c^*) + \alpha^*\,\mathbb{M}a\,\left(p^* + p_{avg}^*\right), \tag{2.26}$$

for which we have: $\mathbf{s}(c) = \left(\dfrac{\rho_0\,\lambda}{L_0^3}\right)\mathbf{s}^*(c^*)$, $\mathbf{q}(p, c) = \left(\dfrac{\rho_0\,g\,b^2}{\eta_0}\right)\mathbf{q}^*(, p^*, c^*)$, $\mu(p, c) = \sigma\,\mu^*(p^*, c^*)$ and $\theta\left(p, c, \dfrac{\partial c}{\partial t}\right) = \left(\dfrac{\rho_0\,q_0}{L_0}\right)\theta^*\left(p^*, c^*, \dfrac{\partial c^*}{\partial t^*}\right)$. In this manner, the first two dimensionless equations in the system (2.21) read:

$$\begin{aligned}
&\nabla^*\cdot\mathbf{q}^*(p^*, c^*) - \frac{\alpha^*}{\mathbb{P}e}\,\Delta^*\mu^*(p^*, c^*) = 0 && \text{in } \Omega^*,\ \forall t^* \in (0, T^*),\\
&\theta^*\left(p^*, c^*, \frac{\partial c^*}{\partial t^*}\right) - \frac{1}{\mathbb{P}e}\,\Delta^*\mu^*(p^*, c^*) && \text{in } \Omega^*,\ \forall t^* \in (0, T^*),
\end{aligned} \tag{2.27}$$

with a straightforward scaling for the boundary and initial conditions. By observing that the dimensionless free energy function $f^*(c^*)$ is:

$$f^*(c^*) = f_0^*(c^*) + \frac{1}{2}\,\mathbb{C}a\,\nabla^* c^* \cdot \nabla^* c^*, \tag{2.28}$$

the dimensionless total free energy $E^* = E^*(p^*, c^*)$ associated to the system (2.21) reads:

$$E^*(p^*, c^*) := \frac{1}{\mathbb{M}a} \int_{\Omega^*} \rho^*(c^*) \left(f^*(c^*) - \mathbb{M}a\,\varphi_p^* \right)\, d\Omega, \tag{2.29}$$

where $E(p, c) = \left(\rho_0\, g\, b\, L_0^3\right)\; E^*(p^*, c^*)$.

For the sake of simplicity, in the rest of the paper, we will omit the superscript $*$ to indicate dimensionless quantities and, otherwise else specified, we will refer only to dimensionless variables and quantities.

Remark 2.1. *The specific discharge* $\mathbf{q}$ *of Eq.* (2.24) *stands for a mass–averaged velocity and is not divergence–free as seen in Eq.* (2.27)*; in addition, the chemical potential* μ *of Eq.* (2.26) *directly depends on the pressure variable* p*. These make the analysis of such Hele–Shaw–Chan–Hilliard formulation quite involved. Conversely, the phase field model of [18] yields a straightforward analysis as it considers a volume–averaged velocity and a modified pressure instead of the physical pressure* p *which, in our model, is unbounded with respect to the interface thickness* $\sqrt{\mathbb{C}a}$*.*

2.5 The sharp interface limit: Darcy flows with discontinuous physical data

By recalling the results of [39, 40], we briefly discuss the sharp interface limit of the Hele–Shaw–Cahn–Hilliard equations. In particular, we are interested in determining the so–called sharp interface model (PDEs) which is obtained from the phase field model it the thickness of the interfaces between the phases tends to zero. The procedure for the derivation of the sharp interface limit is based on the approach of [45] for which asymptotic expansions of the variables p and c in terms of the thickness of the interface are used both far away from the interface (outer expansion) and within the interface (inner expansion); see also [2, 11, 27, 42]. De facto, the investigation of the sharp interface limit constitutes a validation of the phase field model by means of consistency with the interface problem with discontinuous physical data which the model aims at representing through smooth by sharp interfaces. Specifically, the sharp interface model obtained as limit of the Hele–Shaw–Cahn–Hilliard equations is represented by Darcy flows [7] with discontinuous data across an internal interface.

We recall the Darcy equations to model the motion of two immiscible fluids contained in two separated regions (subdomains) Ω_1 and Ω_2 such that $\overline{\Omega}_1 \cup \overline{\Omega}_2 = \overline{\Omega}$ and $\Omega_1 \cap \Omega_2 = \emptyset$ a.e. with an interface $\Gamma := \partial\Omega_1 \cap \partial\Omega_2 \neq \emptyset$; see Fig. 3. Let us observe that when a prescribed phase field variable c is provided and the phases are fully decomposed, the variable c can be used to track the subdomains Ω_i, $i = 1, 2$, and the interface Γ by identifying the locations

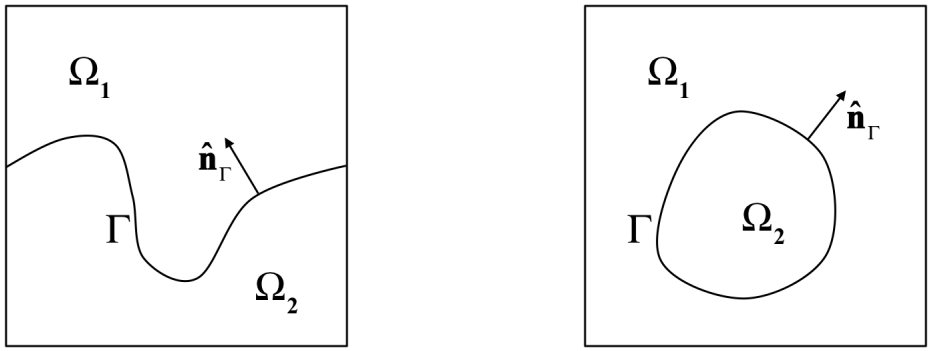

Figure 3: Examples for internal discontinuity interfaces problems: subdomains Ω_1 and Ω_2, interface Γ and unit vector $\hat{\mathbf{n}}_\Gamma$ normal to Γ.

for which $c = c_1$ or $c = c_2$, respectively. For the specific choice of the bulk energy functional (2.7) for which the pure phases corresponds to $c_1 = 1$ and $c_2 = 0$, we can define $\Omega_1 := \left\{\mathbf{x} \in \Omega \ : \ c(\mathbf{x}) > \frac{1}{2}\right\}$, $\Omega_2 := \left\{\mathbf{x} \in \Omega \ : \ c(\mathbf{x}) < \frac{1}{2}\right\}$ and $\Gamma := \left\{\mathbf{x} \in \Omega \ : \ c(\mathbf{x}) = \frac{1}{2}\right\}$. As consequence, for this choice, we have that where $c = c_1 = 1$ we are referring to the subdomain Ω_1 filled with a fluid with density ρ_1 and viscosity η_1; conversely, when $c = c_2 = 0$, we indicate the subdomain Ω_2 with the physical properties ρ_2 and η_2. In each subdomain Ω_i, $i = 1, 2$, we define two variables p_i for the pressure and the fluxes $\overline{\mathbf{q}}_i(p_i)$ such that:

$$\overline{\mathbf{q}}_i(p_i) := -\frac{1}{12\,\eta_i}\left(\nabla p_i + (\rho_{avg} - \rho_i)\,\hat{\mathbf{g}}\right). \tag{2.30}$$

Then, the Darcy model in each subdomain Ω_i, $i = 1, 2$, reads:

$$\nabla \cdot \overline{\mathbf{q}}_i(p_i) = 0 \qquad \text{in } \Omega_i, \tag{2.31}$$

with suitable boundary conditions (Dirichlet, Neumann or Robin) imposed on the the external boundary if $\partial\Omega \cap \partial\Omega_i \neq \emptyset$. If we denote with p the pressure variable in Ω, we have that $p|_{\Omega_i} = p_i$ and similarly $\overline{\mathbf{q}}(p)|_{\Omega_i} = \overline{\mathbf{q}}_i(p_i)$, for $i = 1, 2$. By denoting with $[\![\cdot]\!]_\Gamma$ the jump of a generic variable across the interface Γ and with $\hat{\mathbf{n}}_\Gamma$ the unit vector normal to Γ which, by convention, we assume as outward directed with respect to the subdomain Ω_2 (see Fig. 3), we define the following interface conditions for two immiscible fluids:

$$\begin{aligned} &[\![p]\!]_\Gamma := p_2|_\Gamma - p_1|_\Gamma = \tau\,\kappa, \\ &[\![\overline{\mathbf{q}}(p)]\!]_\Gamma := \left(\overline{\mathbf{q}}_2(p_2)\cdot\hat{\mathbf{n}}_\Gamma\right)|_\Gamma - \left(\overline{\mathbf{q}}_1(p_1)\cdot\hat{\mathbf{n}}_\Gamma\right)|_\Gamma = 0, \end{aligned} \tag{2.32}$$

where τ is a dimensionless surface tension coefficient and κ indicates the signed dimensionless curvature of the interface. Due to the convention chosen for the normal $\hat{\mathbf{n}}_\Gamma$ to the interface Γ, we have that $\kappa := \nabla \cdot \hat{\mathbf{n}}_\Gamma$.

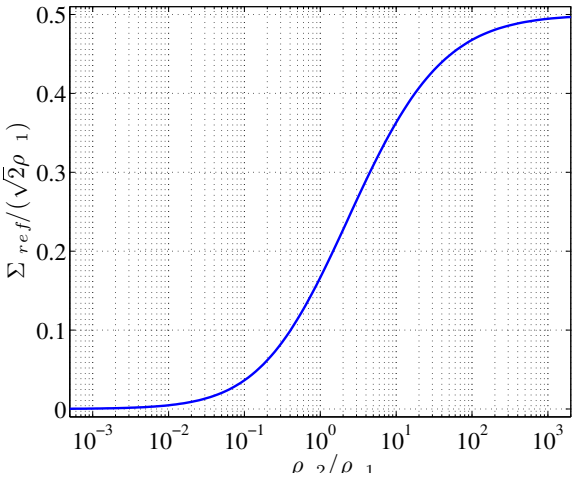

Figure 4: Normalized parameter Σ_{ref} (2.33) $\left(\dfrac{\Sigma_{ref}}{\sqrt{2}\rho_1}\right)$ vs. $\dfrac{\rho_2}{\rho_1}$ for $\rho_1 = 1$, $c_1 = 1$, $c_2 = 0$ and the bulk energy function (2.7).

Remark 2.2. *The interface conditions (2.32) corresponding to the Darcy equations (2.31) represent a particular, but physically consistent case of an internal discontinuity interface problem associated to the Laplace equations defined on the separated subdomains. The latter problem is afforded for example in [19] where the jumps of the variable p and the flux $\overline{\mathbf{q}}(p)$ are set equal to some prescribed generic functions g_p and $g_{\overline{\mathbf{q}}}$ defined on Γ, i.e. $[\![p]\!]_\Gamma = g_p$ and $[\![\overline{\mathbf{q}}(p)]\!]_\Gamma = g_{\overline{\mathbf{q}}}$; for the specific case of Darcy flows, we have $g_p = \tau\,\kappa$ and $g_{\overline{\mathbf{q}}} = 0$. For further details on internal discontinuity interface problems and their numerical approximation we refer the interested reader e.g. to [8, 19].*

Let us indicate with ε the dimensionless characteristic size of the interfaces between the pure phases; specifically we set $\varepsilon = \sqrt{\dfrac{\lambda}{L_0^2}}$. moreover, we introduce the parameter Σ_{ref} defined as [4]:

$$\Sigma_{ref} := \sqrt{2} \int_{c_2}^{c_1} \rho(c) \sqrt{f_0(c) - f_0(c_1) - \frac{df_0}{dc}(c_1)(c - c_1)}\, dc; \tag{2.33}$$

an example of Σ_{ref} is reported in Fig. 4. Following [39, 42] it is possible to show that under the assumption that $\kappa \ll \dfrac{1}{\varepsilon}$ and with the choice of the following scalings in ε for the

[4] As discussed in [42] the value of Σ_{ref} obtained for the cylindrical coordinates tends in the limit to the value obtained for the planar case; for this reason, we consider an unique value of Σ_{ref} for both the cases.

dimensionless parameters [5]:

$$\mathbb{C}a = \varepsilon^2, \quad \mathbb{M}a = \frac{\Sigma_{ref}}{\tau}\,\varepsilon, \quad \text{and} \quad \mathbb{P}e = \frac{1}{\varepsilon}, \tag{2.34}$$

the Hele–Shaw–Cahn–Hilliard equations (2.27) tend, in the sharp interface limit $\varepsilon \to 0$, to the sharp interface model represented by the Darcy equations (2.31) defined in the subdomains Ω_i with the interface conditions (2.32) defined on Γ. In this manner, the Darcy flow problem of two immiscible fluids with discontinuous physical properties can be obtained as the limit of the Hele–Shaw phase field model for the thickness of the interfaces between the pure phases tending to zero. As a consequence, the numerical approximation of the Hele–Shaw–Cahn–Hilliard equations represents a viable, mathematically and thermodynamically consistent approach for the solution of the Darcy flow problem (2.31) with the interface conditions (2.32) without resorting to interface capturing or interface tracking methods, as e.g. the volume of fluid or level set methods [34, 44, 50].

Remark 2.3. *Following the Remark 2.2 and the previous considerations on the sharp interface limit, suitable phase field models coupled with the Cahn–Hilliard equations can be eventually developed to represent generic internal discontinuity interface problems when the interface thickness among the pure phases tends in the limit to zero; see [2, 42].*

2.6 The weak formulation

By using a standard notation to denote the Sobolev spaces of functions with Lebesgue measurable derivatives and norms [3], we define the function spaces:

$$\begin{aligned} \mathcal{V} &:= \left\{ \phi \in H^1(\Omega) \,:\, \int_\Omega \phi \, d\Omega = 0 \text{ and } \phi|_{\Gamma_{in}} = \phi|_{\Gamma_{out}} \right\}, \\ \mathcal{H} &:= \left\{ \psi \in H^2(\Omega) \,:\, \psi|_{\Gamma_{in}} = \psi|_{\Gamma_{out}} \text{ and } (\nabla\psi \cdot \hat{\mathbf{n}})\,|_{\Gamma_{in}} = -\,(\nabla\psi \cdot \hat{\mathbf{n}})\,|_{\Gamma_{out}} \right\}, \end{aligned} \tag{2.35}$$

with $\mathcal{V}$ and $\mathcal{H}$ accounting for the periodic boundary conditions.

We define, for all $t \in (0,T)$, the residuals $R_p(p,c)(\cdot) \,:\, \mathcal{H} \to \mathbb{R}$ and $R_c(p,c)(\cdot) \,:\, \mathcal{H} \in \mathbb{R}$ for given $p \in \mathcal{V}$ and $c \in \mathcal{H}$:

$$R_p(p,c)(\phi) := -\int_\Omega \nabla\phi \cdot \mathbf{q}(p,c)\, d\Omega + \frac{\alpha}{\mathbb{P}e}\, D(p,c)(\phi), \tag{2.36}$$

$$R_c(p,c)(\psi) := \int_\Omega \psi\, \theta\left(p, c, \frac{\partial c}{\partial t}\right) d\Omega + \frac{1}{\mathbb{P}e} D(p,c)(\psi), \tag{2.37}$$

where, by integration by parts and using Eq. (2.26), we have introduced the real–valued form $D(p,c)(\psi)$ for any $\psi \in \mathcal{H}$:

$$\begin{aligned} D(p,c)(\psi) \;:=\; & \int_\Omega \nabla\psi \cdot \nabla\left(\frac{df_0}{dc}(c)\right) d\Omega + \alpha\, \mathbb{M}a \int_\Omega \nabla\psi \cdot \nabla\left(p + p_{avg}\right) d\Omega \\ & + \mathbb{C}a \int_\Omega \Delta\psi\, \frac{1}{\rho(c)} \nabla\cdot(\rho(c)\nabla c)\, d\Omega. \end{aligned} \tag{2.38}$$

[5] The Péclet number can be also set as independent of ε, specifically we can take $\mathbb{P}e = 1$ [39]. The scaling for the parameter $\mathbb{M}a$ corresponds to the choice of the dimensional surface tension coefficient $\sigma = (g\,L_0)\,\dfrac{\tau}{\Sigma_{ref}}\,\dfrac{1}{\varepsilon}$.

Finally, the weak formulation of the Hele–Shaw–Cahn–Hilliard equations reads:

$$\begin{aligned} &\text{find, for almost all } t \in (0,T),\ p \in \mathcal{V} \text{ and } c \in \mathcal{H}\ : \\ &\quad R_p(p,c)(\phi) = 0 \qquad \forall \phi \in \mathcal{H}, \\ &\quad R_c(p,c)(\psi) = 0 \qquad \forall \psi \in \mathcal{H}, \\ &\quad \text{with } c = c_0 \qquad \text{in } \Omega,\ t = 0. \end{aligned} \tag{2.39}$$

We notice that the choice of the function space $\mathcal{H}$ for the weight function ϕ in Eq. (2.36) and the first of the equations (2.39) is due to the second order derivatives in the form $D(p,c)(\phi)$ of Eq. (2.38).

3 Numerical Approximation

We discuss the numerical solution of problem (2.39) both in terms of the spatial and time approximations which are based on Isogeometric Analysis and the generalized–α method, respectively. For alternative formulations, we refer the reader to [23, 24, 40, 54].

3.1 The spatial approximation: Isogeometric Analysis

For the spatial approximation of problem (2.39) we consider Isogeometric Analysis [15, 35]. Since the solution field $c \in \mathcal{H} \subset H^2(\Omega)$ for all $t \in (0,T)$, it is necessary to approximate it with at least globally C^1–continuous basis functions; see [51] and e.g. [6, 17, 28, 30, 41]. For the sake of simplicity, despite the fact that only globally C^0–continuous basis functions are necessary for the approximation of the pressure field $p \in \mathcal{V} \subset H^1(\Omega)$, we use the same basis functions for both the pressure and phase fields.

We introduce the multivariate B–splines (NURBS) basis $\mathbf{N}(\mathbf{x}) := \{N_A(\mathbf{x})\}_{A=1}^{n_{bf}}$ which is composed by n_{bf} basis functions [46]. Then, we write the approximate pressure $p_h = p_h(t,\mathbf{x})$ and phase $c_h = c_h(t,\mathbf{x})$ fields as $p_h(t,\mathbf{x}) = \sum_{A=1}^{n_{bf}} p_A(t)\, N_A(\mathbf{x})$ and $c_h(t,\mathbf{x}) = \sum_{A=1}^{n_{bf}} c_A(t)\, N_A(\mathbf{x})$, respectively, with the coefficients $\{p_A(t)\}_{A=1}^{n_{bf}}$ and $\{c_A(t)\}_{A=1}^{n_{bf}}$ being time dependent; similarly, for the test functions, we choose $\phi_h(\mathbf{x}) = \sum_{A=1}^{n_{bf}} \phi_A\, N_A(\mathbf{x})$ and $\psi_h(\mathbf{x}) = \sum_{A=1}^{n_{bf}} \psi_A\, N_A(\mathbf{x})$. More specifically, we introduce the discrete function spaces $\mathcal{V}_h \subset \mathcal{V}$ and $\mathcal{H}_h \subset \mathcal{H}$ composed of basis functions of local degree $p = 2$ and such that the periodic boundary conditions are included [6]; the reader interested to a discussion about the strong imposition of periodic boundary conditions in the field of Isogeometric Analysis is referred to e.g. [6, 41]. We indicate with $n_{h,p}$ the dimension of the space $\mathcal{V}_h$ and with $n_{h,c}$ the dimension of $\mathcal{H}_h$; we

[6] The requirement of a zero mean value for the pressure field is replaced by setting equal to zero a control variable of the approximate pressure field.

observe that, due to the previous considerations and the definition of the space $\mathcal{V}$, we have that $n_{h,p} = n_{h,c} - 1$.

The semi–discrete version of the weak problem (2.39) reads:

$$\begin{aligned} &\text{find, for all } t \in (0,T),\ p_h \in \mathcal{V}_h \text{ and } c_h \in \mathcal{H}_h\ : \\ &\qquad R_p(p_h, c_h)(\phi_h) = 0 \qquad \forall \phi_h \in \mathcal{H}_h, \\ &\qquad R_c(p_h, c_h)(\psi_h) = 0 \qquad \forall \psi \in \mathcal{H}_h, \\ &\qquad \text{with } c_h = c_{0,h} \qquad \text{in } \Omega,\ t = 0, \end{aligned} \tag{3.1}$$

where $c_{0,h}$ is the L^2 projection of the initial condition c_0 onto the space $\mathcal{H}_h$; the total number of spatial degrees of freedom is $n_h := n_{h,p} + n_{h,c}$ (or equivalently $n_h = 2\, n_{h,c} - 1$).

In view of the time approximation it is convenient to express also the residuals in terms of time derivative of the approximate phase field, say $\dot{c}_h := \dfrac{\partial c_h}{\partial t}$ for the sake of simplicity. We define $\mathbf{P}(t) := \{p_A(t)\}_{A=1}^{n_{bf}}$, $\mathbf{C}(t) := \{c_A(t)\}_{A=1}^{n_{bf}}$, and $\dot{\mathbf{C}}(t) := \{\dot{c}_A(t)\}_{A=1}^{n_{bf}}$, and, from Eqs. (2.36) and (2.37), the residuals:

$$\begin{aligned} &\mathbf{R}_p\left(\mathbf{P}(t), \mathbf{C}(t)\right) := \left\{R_p\left(p_h, c_h\right)\left(N_A\right)\right\}_{A=1}^{n_{bf}}, \\ &\mathbf{R}_c\left(\mathbf{P}(t), \mathbf{C}(t), \dot{\mathbf{C}}(t)\right) := \left\{R_c\left(p_h, c_h\right)\left(N_A\right)\right\}_{A=1}^{n_{bf}}. \end{aligned} \tag{3.2}$$

Since in this work we consider B–splines (NURBS) basis of degree $p = 2$ which are globally C^1–continuous, a 3×3 Gauss–Legendre quadrature rule is used in each element.

3.2 The time approximation: generalized–α method

For the time approximation of the semi–discrete problem (3.1) we consider the generalized–α method [14, 38]; we outline the numerical approach and, for a more detailed description, we refer the reader to [17, 28].

We partition the whole time interval $[0, T]$ into n_{ts} time steps of size $\Delta t_n := t_{n+1} - t_n$, with $\{t_n\}_{n=0}^{n_{ts}}$ the discrete time vector, for which the discrete variables read $\mathbf{P}_n = \mathbf{P}(t_n)$, $\mathbf{C}_n = \mathbf{C}(t_n)$ and $\dot{\mathbf{C}}_n = \dot{\mathbf{C}}(t_n)$. Given the variables $\mathbf{C}_n$ and $\dot{\mathbf{C}}_n$ at the time t_n, the generalized–α method consists in solving the following problem at the time step t_{n+1}:

$$\begin{aligned} &\text{find } \mathbf{P}_{n+1},\ \mathbf{C}_{n+1},\ \dot{\mathbf{C}}_{n+1},\ \mathbf{C}_{n+\alpha_f},\ \dot{\mathbf{C}}_{n+\alpha_m}\ : \\ &\qquad \mathbf{R}_p\left(\mathbf{P}_{n+1}, \mathbf{C}_{n+\alpha_f}\right) = \mathbf{0}, \\ &\qquad \mathbf{R}_c\left(\mathbf{P}_{n+1}, \mathbf{C}_{n+\alpha_f}, \dot{\mathbf{C}}_{n+\alpha_m}\right) = \mathbf{0}, \\ &\qquad \mathbf{C}_{n+1} = \mathbf{C}_n + \Delta t_n \dot{\mathbf{C}}_n + \delta \Delta t_n \left(\dot{\mathbf{C}}_{n+1} - \dot{\mathbf{C}}_n\right), \\ &\qquad \mathbf{C}_{n+\alpha_f} = \mathbf{C}_n + \alpha_f \left(\mathbf{C}_{n+1} - \mathbf{C}_n\right), \\ &\qquad \dot{\mathbf{C}}_{n+\alpha_m} = \dot{\mathbf{C}}_n + \alpha_m \left(\dot{\mathbf{C}}_{n+1} - \dot{\mathbf{C}}_n\right), \end{aligned} \tag{3.3}$$

with the residuals given in Eq. (3.2). For the parameters α_m, α_f and $\delta \in \mathbb{R}$ we choose $\alpha_m = \frac{1}{2}\left(\frac{3-\rho_\infty}{1+\rho_\infty}\right)$, $\alpha_f = \frac{1}{1+\rho_\infty}$, and $\delta = \frac{1}{2} + \alpha_m - \alpha_f$, with $\rho_\infty \in [0,1]$ the spectral radius of the amplification matrix at $\Delta t_n \to \infty$ [38]; specifically, we choose $\rho_\infty = 0.5$. We solve the problem (3.3) for $n = 0, \ldots, n_{ts} - 1$ with a predictor–multicorrector scheme, similarly to [17, 41]. The associated linear system is solved by means of the GMRES method [48] preconditioned by an Algebraic Multigrid algorithm with Smoothed Aggregation [26]; the stopping criterion is based on the relative residual with the tolerance 10^{-6}.

4 Numerical Results

We provide and discuss numerical results for the Hele–Shaw–Cahn–Hilliard equations. First, we numerically analyze the sharp interface limit with discontinuous physical data of Sec. 2.5 in the one–dimension. Then, we provide an example of the numerical solution of the Hele–Shaw–Cahn–Hilliard problem in the two–dimensional setting, specifically the so–called "rising bubble" problem driven by two phases with different densities.

4.1 The sharp interface limit under mesh refinement

We consider the numerical approximation of the steady pressure equation (2.39) in one–dimension, both in Cartesian and radial coordinates, for a prescribed distribution of the phase variable, say $\overline{c}$, in $\Omega = (0,1)$. Specifically, the problem reads:

$$\text{find } p \in \overline{\mathcal{V}} \quad : \quad R_p(p, \overline{c})(\phi) = 0 \quad \forall \phi \in \overline{\mathcal{H}}, \tag{4.1}$$

where $\overline{\mathcal{V}} := \left\{\phi \in H^1(\Omega) \ : \ \phi(1) = 0\right\}$ and $\overline{\mathcal{H}} := \left\{\psi \in H^2(\Omega) \ : \ \phi(1) = 0\right\}$ and the spatial differential operators are expressed in Cartesian or radial coordinates; consequently, the unit vector $\hat{\mathbf{g}}$ is identified as $\hat{\mathbf{x}}$ or $\hat{\mathbf{r}}$. The prescribed phase variable assumes the form:

$$\overline{c}(s) = \frac{1}{2}\left[1 + \tanh\left(\frac{s - s_0}{\sqrt{2\,\mathbb{C}a}}\right)\right], \tag{4.2}$$

where the independent variable s represents the Cartesian (x) or radial (r) coordinate, $s_0 \in \Omega$ and $\mathbb{C}a$ is the Cahn number introduced in Eq. (2.22) [7].

By noticing that Eq. (4.1) is linear in the pressure variable, we solve the steady problem by using the Isogeometric spatial approximation outlined in Sec. 3.1. moreover, by following the paradigm introduced in [28] and used in [30, 17, 41], we relate the interface thickness ε to the dimensionless characteristic mesh size, say h, through a safety coefficient $\gamma_s > 0$; specifically, we assume:

$$\varepsilon = \gamma_s\, h; \tag{4.3}$$

a typical and effective choice of the safety parameter is $\gamma_s = 2$. This choice leads to interfaces between the pure phases to become sharper and shaper as the mesh size reduces, thus allowing to explore the sharp interface limit of the pressure equation.

[7] The prescribed phase distribution $\overline{c}$ of Eq. (4.2) solves the steady Cahn–Hilliard equation with suitable boundary conditions; its expression is compatible with the bulk energy function $f_0(c)$ given in Eq. (2.7).

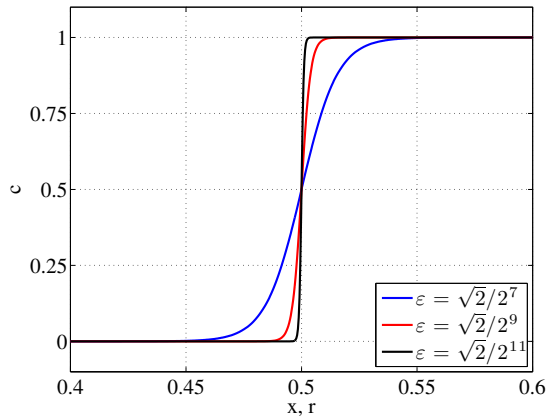

(a) $\overline{c}$(x), $\overline{c}$(r)

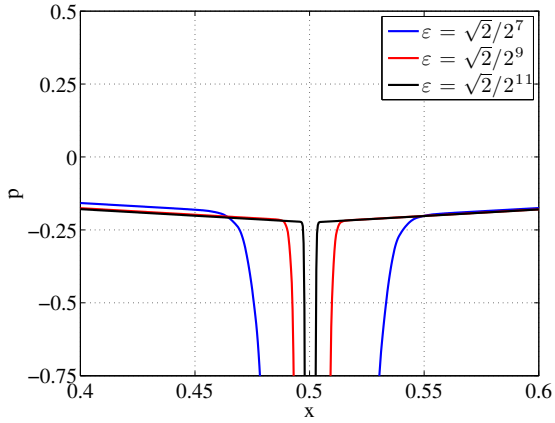

(b) p_h(x), $\tau = 0.5$, $\rho_1 = 1.0$, $\rho_2 = 0.1$

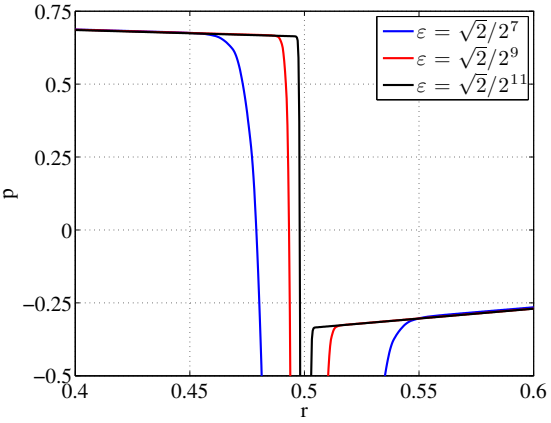

(c) p_h(r), $\tau = 0.5$, $\rho_1 = 1.0$, $\rho_2 = 0.1$

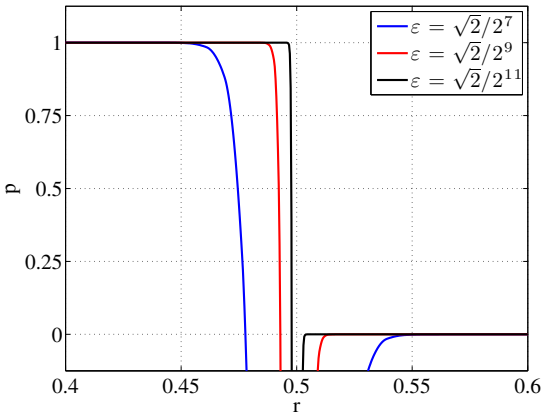

(d) p_h(r), $\tau = 0.5$, $\rho_1 = 1.0$, $\rho_2 = 1.0$

Figure 5: One–dimensional case. Phase variable $\overline{c}$ (a) and pressure distributions p_h (b,c,d) for different values of τ, ρ_2 and ρ_1 in Cartesian x (a,b) and radial coordinates r (a,c,d); zoom around interfaces for $\varepsilon = \dfrac{\sqrt{2}}{2^7}$ (blue), $\dfrac{\sqrt{2}}{2^9}$ (red) and $\dfrac{\sqrt{2}}{2^{11}}$ (black).

In Fig. 5(a) we report the prescribed phase variable $\overline{c}$ both in Cartesian and radial coordinates for uniform meshes of size $h = \dfrac{1}{2^7}$, $\dfrac{1}{2^9}$, and $\dfrac{1}{2^{11}}$ with the interface Γ located in $s_0 = 0.5$ ($\Gamma = \{s_0\}$. In Figs. 5(b,c,d) we highlight the pressure variable p_h around the interfaces for different data. In Fig. 5(a) we consider the Cartesian coordinate with $\tau = 0.5$, $\rho_1 = 1$ and $\rho_2 = 0.1$; as expected the jump of the pressure across the interface tends for $\varepsilon \longrightarrow 0$ to $[\![p]\!]_\Gamma = 0$, being the curvature $\kappa = 0$, while the jump of the derivative of the pressure $\left[\!\left[\dfrac{dp}{d\mathrm{x}}\right]\!\right]_\Gamma = \rho_2 - \rho_1 = -0.9$. In Fig. 5(c) we report the result for the same data, but in radial coordinates; in this case, being the curvature of the interface $\kappa = \dfrac{1}{s_0} = 2.0$, the

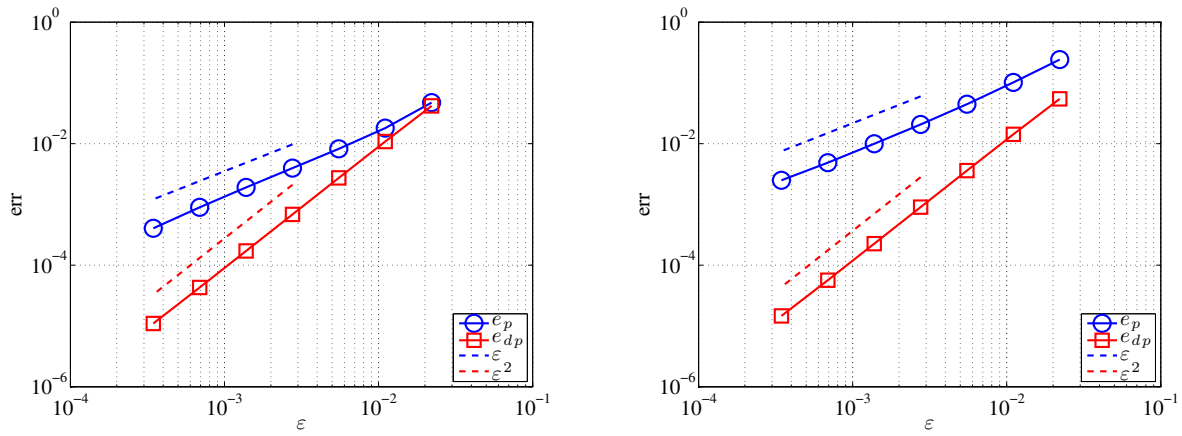

Figure 6: One–dimensional case. Errors e_p and e_{dp} vs. ε for $\tau = 0.5$, $\rho_1 = 1.0$ and $\rho_2 = 0.1$ in Cartesian coordinate (left) and for $\tau = 1.0$, $\rho_1 = 1.0$ and $\rho_2 = 0.05$ in radial coordinate (right).

jump of the pressure tends in the limit to $[\![p]\!]_\Gamma = 1.0$, while $\left[\!\left[\dfrac{dp}{dr}\right]\!\right]_\Gamma = \rho_2 - \rho_1 = -0.9$.

In order to evaluate the convergence orders of the pressure and pressure gradients jumps across the interfaces, we introduce the following notions of jumps, dependent on ε:

$$[\![p_h]\!]_\varepsilon := p_h(s_2^\varepsilon) - p_h(s_1^\varepsilon) \quad \text{and} \quad \left[\!\left[\frac{dp_h}{ds}\right]\!\right]_\varepsilon := \frac{dp_h}{ds}(s_2^\varepsilon) - \frac{dp_h}{ds}(s_1^\varepsilon), \tag{4.4}$$

where $s_1^\varepsilon := \underset{s\in\Omega}{\text{argsup}}\,\{\overline{c}(s) \ : \ \overline{c}(s) \le c_1 - tol\}$ and $s_2^\varepsilon := \underset{s\in\Omega}{\text{arginf}}\,\{\overline{c}(s) \ : \ \overline{c}(s) \ge c_2 + tol\}$, for $c_2 < c_1$ and some tolerance $tol_\varepsilon > 0$; specifically, for the one–dimensional case, we set $c_1 = 1$, $c_2 = 0$, and $tol = 10^{-10}$. We compute the errors associated to the jumps $[\![p_h]\!]_\varepsilon$ and $\left[\!\left[\dfrac{dp_h}{ds}\right]\!\right]_\varepsilon$ of Eq. (4.4), say e_p and e_{dp}, as:

$$e_p := |\,[\![p_h]\!]_\varepsilon - [\![p]\!]_\Gamma\,| \quad \text{and} \quad e_{dp} := \left|\,\left[\!\left[\frac{dp_h}{ds}\right]\!\right]_\varepsilon - \left[\!\left[\frac{dp}{ds}\right]\!\right]_\Gamma\,\right|, \tag{4.5}$$

respectively.

In Fig. 6, we report the errors e_p and e_{dp} on the pressure and pressure gradient jumps across the interface vs. the parameter ε for two test problems; in the first case, the Cartesian coordinate is used with $\tau = 0.5$, $\rho_1 = 1.0$, and $\rho_2 = 0.1$, for which $[\![p]\!]_\Gamma = 0$ and $\left[\!\left[\dfrac{dp}{\mathrm{dx}}\right]\!\right]_\Gamma = -0.9$, while in the second case, which is in radial coordinate, $\tau = 1.0$, $\rho_1 = 1.0$, and $\rho_2 = 0.05$, yielding $[\![p]\!]_\Gamma = 1.0$ and $\left[\!\left[\dfrac{dp}{dr}\right]\!\right]_\Gamma = -0.95$. We remark that the error e_p on the pressure jump converges to zero with order 1 in ε, while the error e_{dp} on the jump of the pressure gradient converges to zero with order 2 for both the test problems.; the same convergence orders are

obtained for spatial discretizations with B–splines basis functions of degree $r > 2$, which are at least globally C^1–continuous. Indeed, such results correspond to an intrinsic property of the sharp interface limit (Sec. 2.5) obtained for the specific Hele–Shaw–Cahn–Hilliard model at hand ([39]); for more details, we refer the reader to [18] and the analysis therein, which exploits the sharp asymptotic limit for high order terms in ε. From this result, extendable to the two– and three–dimensional cases, we deduce that the pressure equation (4.1), endowed with a prescribed phase field variable $\bar{c}$, solves a Poisson problem in p with conditions on the jumps of the pressure and gradient of the pressure across an internal interface Γ in Ω.

4.2 Discontinuous density: the "rising bubble" problem

We consider the case of a "rising bubble", i.e. a phase comprised of a "light" fluid (phase 1) embedded in an heavier one (phase 2), which rises in presence of the gravitational force [36]; as computational domain, we choose $\Omega = (0,1)^2$. We select the following parameters introduced in Sec. 2: $\rho_1 = 5.8507$, $\rho_2 = 14.8507$, $\eta_1 = \eta_2 = 0.5$, $\sigma = 73.186$, $\tau = 0.235702$, $g = 9.81$, and $\epsilon = 1/64$; we deduce that $\Sigma_{ref} = 2.0213$ from Eq. (2.33), $\mathbb{C}a = 0.000244141$, $\mathbb{M}a = 0.133994$, and $\mathbb{P}e = 320$ from Eq. (2.34). The initial condition for the phase field is $c_0(\mathrm{x},\mathrm{y}) = \dfrac{1}{4}\,\zeta_+(\mathrm{x},\mathrm{y})\,\zeta_-(\mathrm{x},\mathrm{y})$, where $\zeta_\pm(\mathrm{x},\mathrm{y}) = 1 + \tanh\left(\dfrac{\mathrm{y} - \mathrm{y}_\pm(\mathrm{x})}{\sqrt{2\,\mathbb{C}a}}\right)$, being $\mathrm{y}_\pm(\mathrm{x}) = \dfrac{1}{2} \pm \dfrac{5 + \cos(2\pi\mathrm{x})}{20\,\pi}$; this choice determines the distribution of the "light" and "heavy" fluids shown in Fig. 7(top–left) which are depicted in red and blue, respectively. We remark that periodic type boundary conditions are used.

We solve the problem by means of IGA with B–splines basis functions of degree 2 and globally C^1–continuous in Ω; specifically, we select a uniform mesh of size $h = 1/128$ yielding a number of basis functions $n_{bf} = 16'384$. For the time discretization, we use the generalized–α method as described in Sec. 3.2 with $\Delta t = 5.0 \cdot 10^{-4}$.

We report in Figs. 7–9 the phase field variable c at different times and, correspondingly in Figs. 10–12, the pressure field p. We highlight that the "light" fluid raises in the heavier one and the initial condition c_0 determines the pinch–off of the stratified fluid distribution up to the generation of a bubble; the solution exhibits a topological change that is taken into account from the phase field model in a straightforward fashion. Similarly, the pressure p highlights the mechanism driving this topological change and the consequent rise of the "light" bubble into the "heavy" fluid.

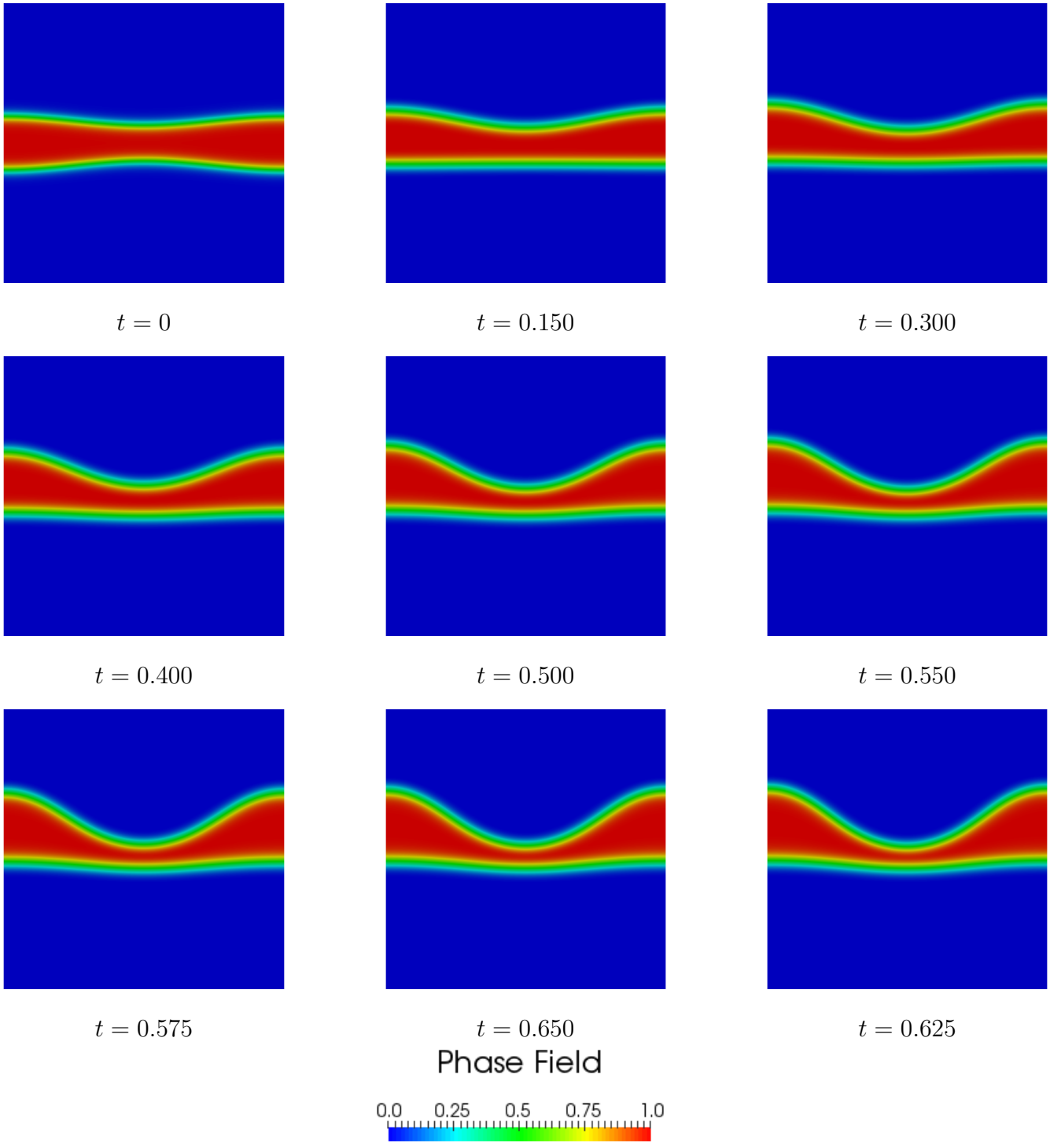

Figure 7: "Rising bubble": phase variable c at different time instances.

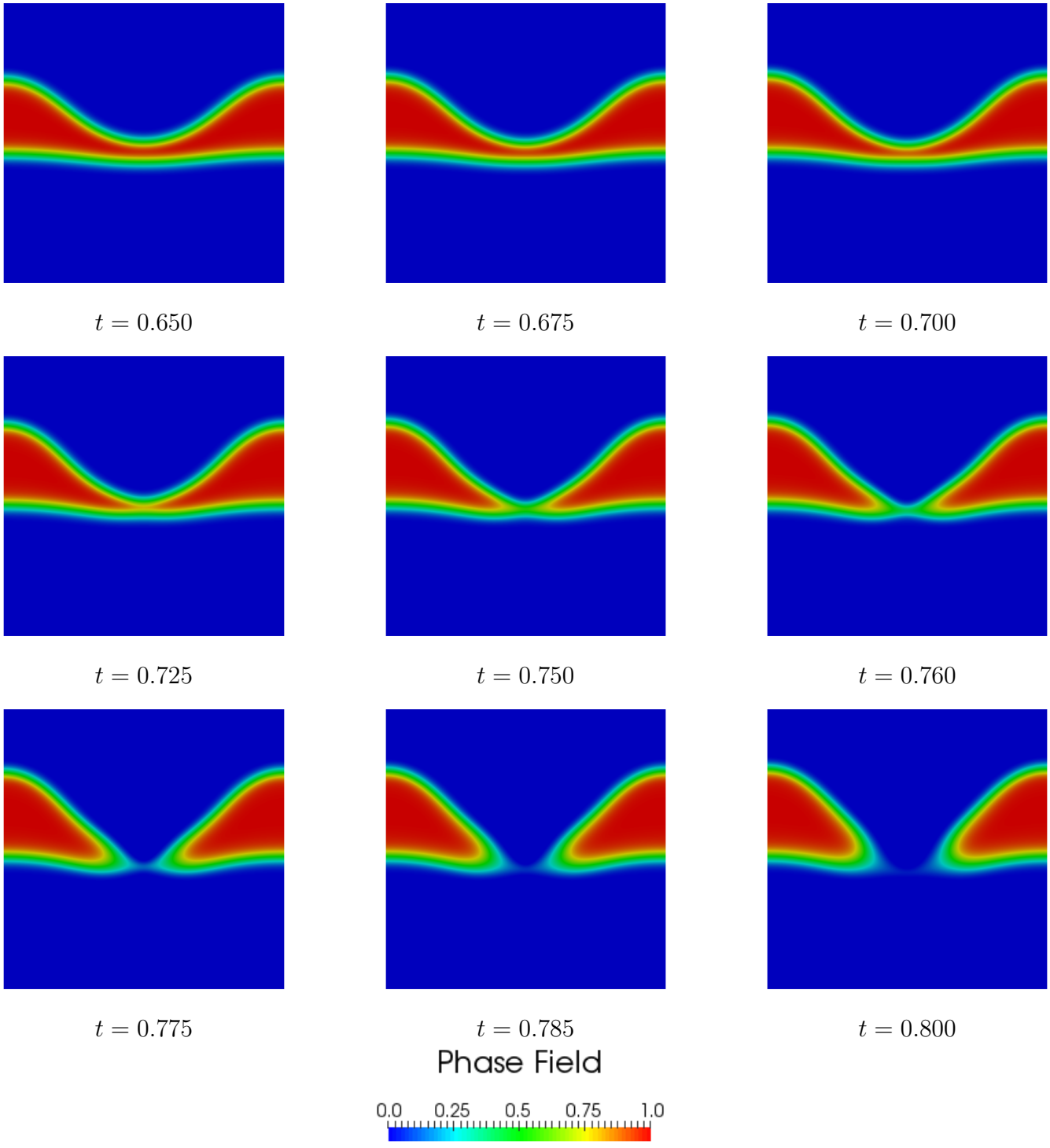

Figure 8: "Rising bubble": phase variable c at different time instances.

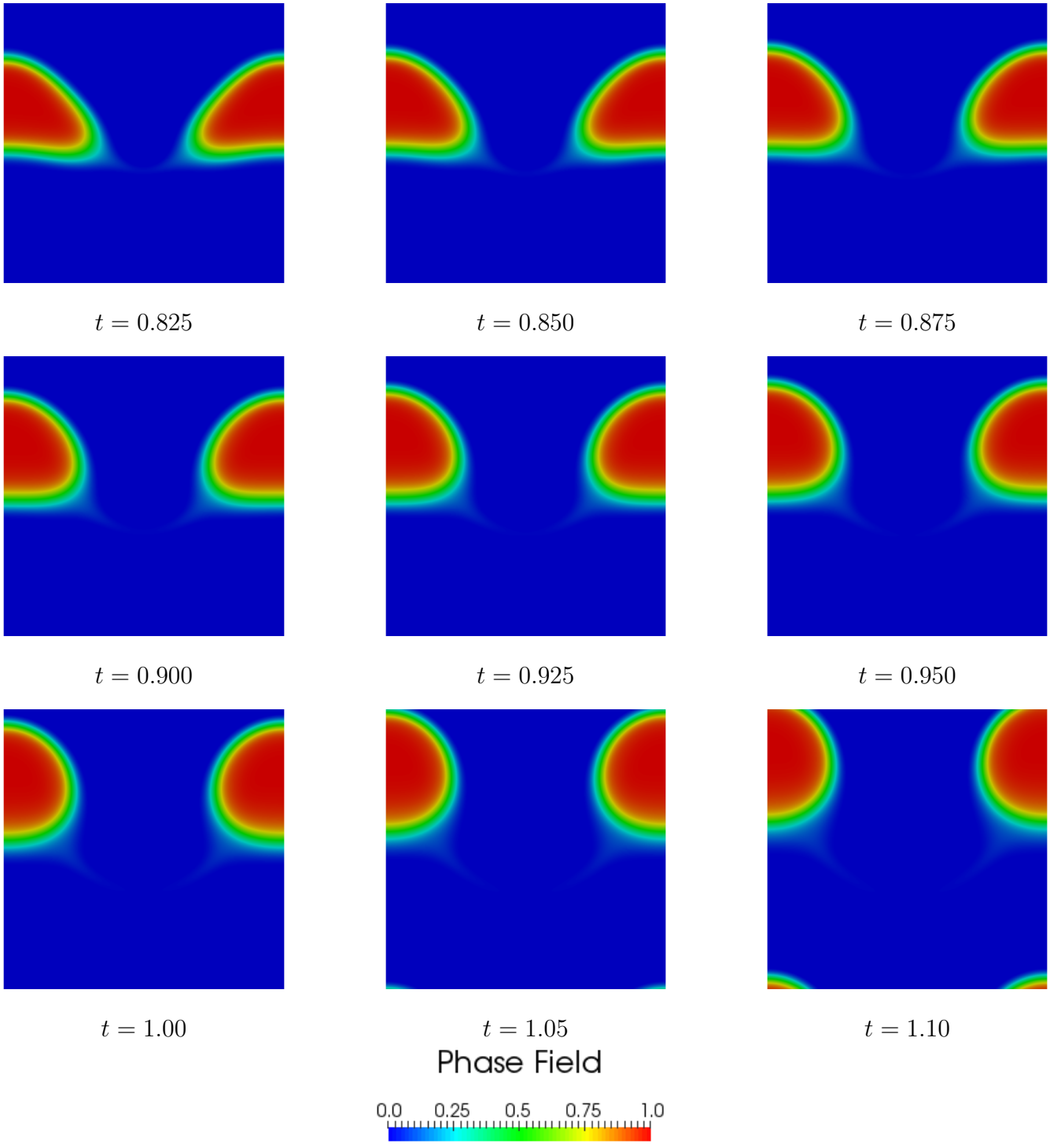

Figure 9: "Rising bubble": phase variable c at different time instances.

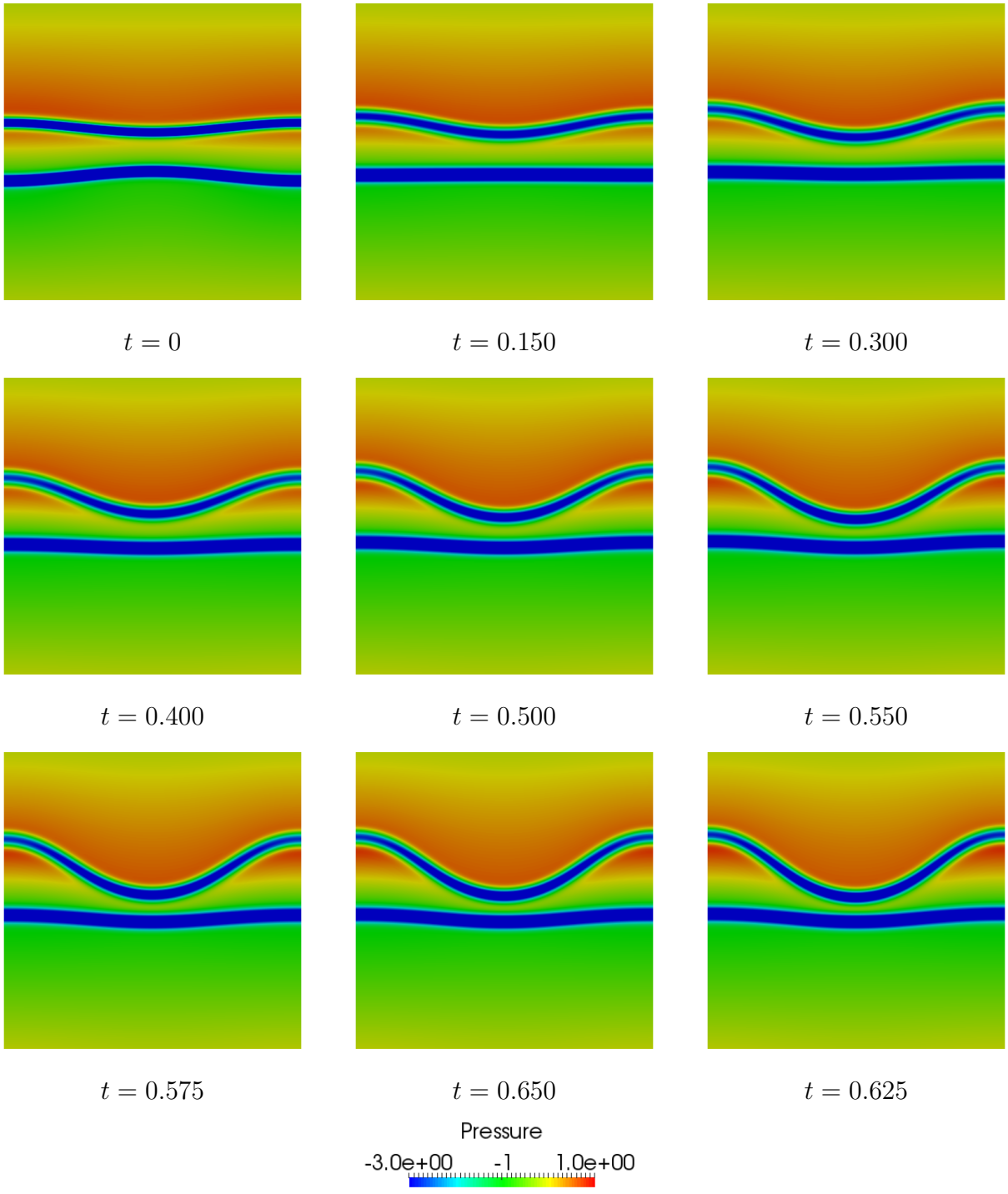

Figure 10: "Rising bubble": pressure p at different time instances.

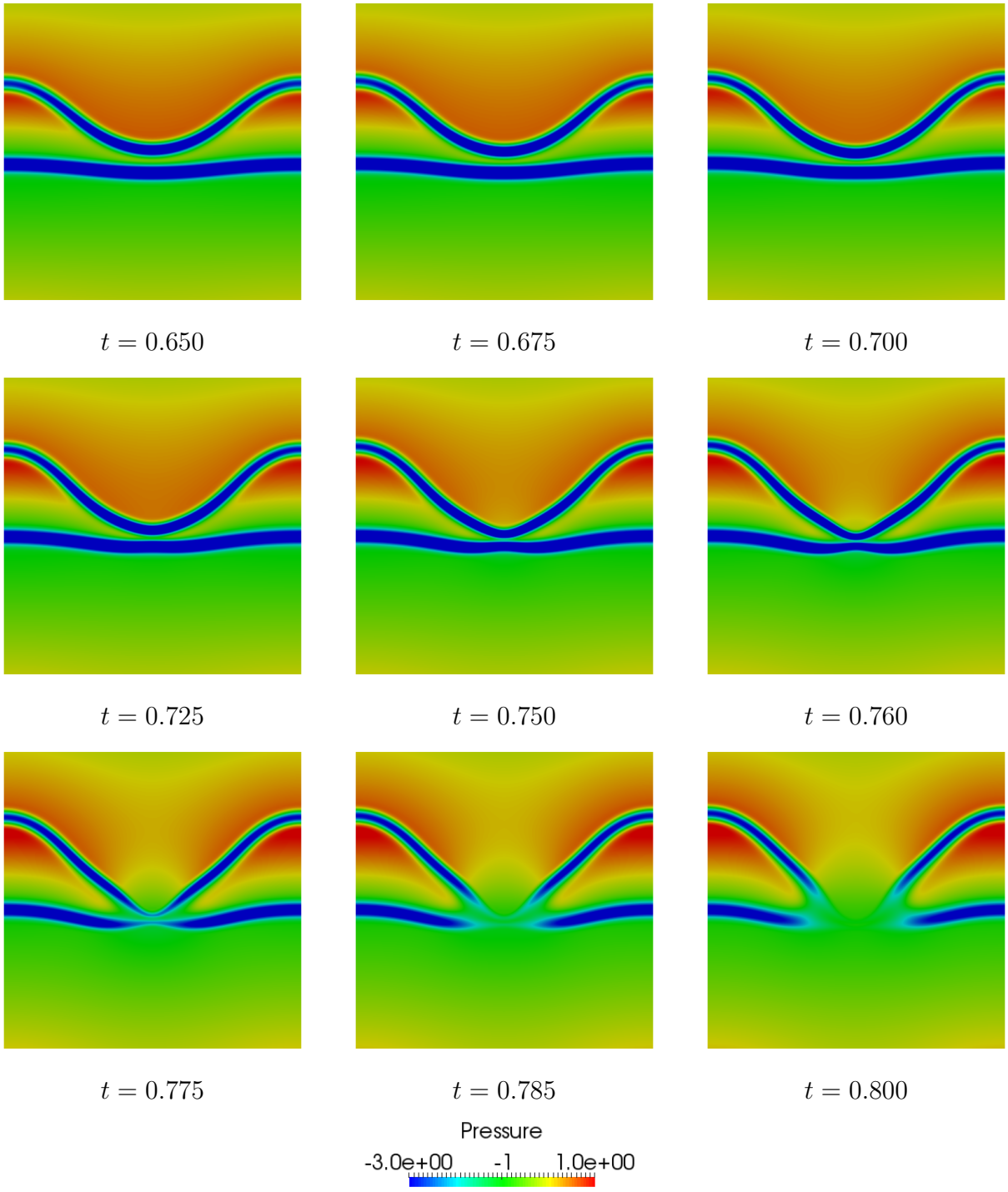

Figure 11: "Rising bubble": pressure p at different time instances.

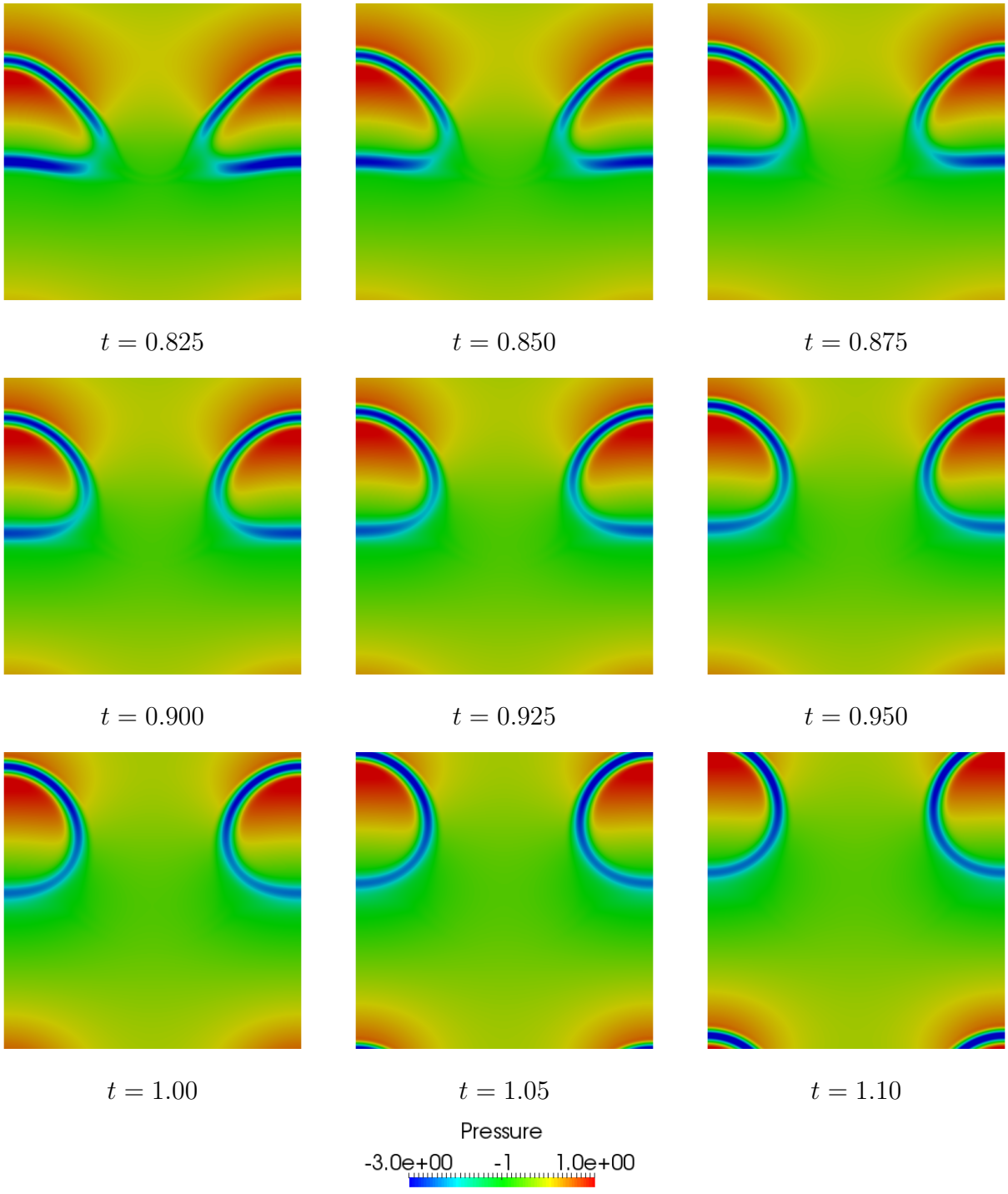

Figure 12: "Rising bubble": pressure p at different time instances.

5 Conclusions

In this paper, we considered Isogeometric Analysis for the spatial approximation of the Hele–Shaw–Cahn–Hilliard equations, a phase field model particularly useful to represent Darcy flows in a two–dimensional cell in presence of discontinuous data through interfaces. We showed that our numerical formulation is suitable and efficient for approximating this model by solving the benchmark "rising bubble" problem of fluids with different densities in presence of the gravitational force. In addition, we numerically verified the sharp interface limit of the Hele–Shaw–Cahn–Hilliard equations which is represented by Poisson problems in the pressure variable across interfaces and endowed with interface conditions to match discontinuities in the data. Specifically, these interface conditions are jump conditions on the pressure and its gradient and are proportional to the surface tension and the density gap across the interface, respectively. Our numerical tests showed that the pressure equation of the Hele–Shaw–Cahn–Hilliard equations can also be used to model internal discontinuity interface Poisson problems by prescribing a suitable phase field variable in the computational domain to represent interfaces.

Acknowledgements

The authors acknowledge Prof. H. Garcke, Dr. K.F. Lam (University of Regensburg), and Prof. S. Salsa (Politecnico di Milano) for the fruitful discussions and insights into the topic.

References

[1] Global weak solutions and asymptotic limits of a Cahn–Hilliard–Darcy system modelling tumour growth. *AIMS Mathematics*, 1(Math-01-00318, pages =).

[2] H. Abels, H. Garcke, and G. Grün. Thermodynamically consistent, frame indifferent diffuse interface models for incompressible two-phase flows with different densities. *Mathematical Models and Methods in Applied Sciences*, 22(03):1150013, 2012.

[3] R.A. Adams. *Sobolev Spaces*. Academic Press, New York, 1975.

[4] I. Akkerman, Y. Bazilevs, C.E. Kees, and M.W. Farting. Isogeometric analysis of free–surface flow. *Journal of Computational Physics*, 230(11):4137–4152, 2011.

[5] J.W. Barrett, J.F. Blowey, and H. Garcke. Finite element approximation of the Cahn-Hilliard equation with degenerate mobility. *SIAM Journal on Numerical Analysis*, 37(1):286–318, 1999.

[6] A. Bartezzaghi, L. Dedè, and A. Quarteroni. Isogeometric analysis of high order partial differential equations on surfaces. *Computer Methods in Applied Mechanics and Engineering*, 295(Supplement C):446–469, 2015.

[7] J. Bear. *Dynamics of Fluids in Porous Media*. Dover Publications, Mineola, NY, 1988.

[8] T. Belytschko, N. Moes, S. Usui, and C. Parimi. Aribitrary discontinuities in finite elements. *International Journal for Numerical Methods in Engineering*, 50(4):993–1013, 2001.

[9] S. Bosia, M. Conti, and M. Grasselli. On the Cahn–Hilliard–Brinkman system. *Communications in Mathematical Sciences*, 13(6):1541–1567, 2015.

[10] L.A. Caffarelli and N.E. Muler. An L^∞ bound for solutions of the Cahn–Hilliard equation. *Archive for Rational Mechanics and Analysis*, 133(2):457–487, 1995.

[11] G. Caginalp. Stefan and Hele–Shaw type models as asymptotic limits of the phase–field equations. *Physical Review A*, 39(11):5587–5896, 1989.

[12] J.W. Cahn. On spinodal decomposition. *Acta Metallica*, 9(9):795–801, 1961.

[13] J.W. Cahn and J.E. Hilliard. Free energy of a nonuniform system. I. Interfacial free energy. *Journal of Chemical Physics*, 28(2):258–267, 1958.

[14] J. Chung and G.M. Hulbert. A time integration algorithm for structural dynamics with improved numerical dissipation: The generalized–α method. *Journal of Applied Mechanics*, 60(2):371–375, 1993.

[15] J.A. Cottrell, T.J.R. Hughes, and Y. Bazilevs. *Isogeometric Analysis: Towards Integration of CAD and FEA*. John Wiley and Sons, 2009.

[16] L. Cueto-Felgueroso and R. Juanes. A phase–field model of unsaturated flow. *Water Resources Research*, 45:W10409, 2009.

[17] L. Dedè, M.J. Borden, and T.J.R. Hughes. Isogeometric analysis for topology optimization problems in a phase field approach. *Archives of Computational Methods in Engineering*, 19(3):427–465, 2012.

[18] L. Dedè, H. Garcke, and K.F. Lam. A Hele–Shaw–Cahn–Hilliard model for incompressible two–phase flows with different densities. *Journal of Mathematical Fluid Mechanics*, Jul 2017.

[19] M. Discacciati, A. Quarteroni, and S. Quinodoz. Numerical approximation of internal discontinuity interface problems. *SIAM Journal on Scientific Computing*, 35(5):A2341–A2369, 2013.

[20] C.M. Elliott and H. Garcke. On the Cahn–Hilliard equation with degenerate mobility. *SIAM Journal on Mathematical Analysis*, 27(2):404–423, 1996.

[21] M. Fei. Global sharp interface limit of the Hele–Shaw–Cahn–Hilliard system. *Mathematical Methods in the Applied Sciences*, 40(3):833–852, 2017.

[22] X. Feng. Fully discrete finite element approximations of the Navier–Stokes–Cahn–Hilliard diffuse interface model for two–phase fluid flows. *SIAM Journal on Numerical Analysis*, 44(3):1049–1072, 2006.

[23] X. Feng and S.M. Wise. Analysis of a Darcy–Cahn–Hilliard diffuse interface model for the Hele–Shaw flow and its fully discrete finite element approximation. *SIAM Journal on Numerical Analysis*, 50(3):13201343, 2013.

[24] X. Feng and H. Wu. A posteriori error estimates for finite element approximations of the Cahn–Hilliard equation and Hele–Shaw flow. *Journal of Computational Mathematics*, 26(6):767–796, 2008.

[25] P.C. Fife. Models for phase separation and their mathematics. *Electronic Journal of Differential Equations*, 48:1–26, 2000.

[26] M.W. Gee, C.M. Siefert, J.J. Hu, R.S. Tuminaro, and M.G. Sala. Ml 5.0 smoothed aggregation user's guide. Technical Report SAND2006–2649, Sandia National Laboratories, 2006.

[27] K. Glasner. A diffuse interface approach to Hele–Shaw flow. *Nonlinearity*, 16(1):49–66, 2003.

[28] H. Gómez, V.M. Calo, Y. Bazilevs, and T.J.R. Hughes. Isogeometric analysis of the Cahn–Hilliard phase–field model. *Computer Methods in Applied Mechanics and Engineering*, 197(49-50):4333–4352, 2008.

[29] H. Gómez and T.J.R. Hughes. Provably unconditionally stable, second–order time accurate, mixed variational methods for phase–field models. *Journal of Computational Physics*, 230(13):5310–5327, 2011.

[30] H. Gómez, T.J.R. Hughes, X. Nogúeira, and V.M. Calo. Isogeometric analysis of the Navier–Stokes–Korteweg equations. *Computer Methods in Applied Mechanics and Engineering*, 199(25-28):1828–1840, 2010.

[31] S. Gross and A. Reusken. *Numerical Methods for Two–Phase Incompressible Flows*. Springer, Berlin, 2011.

[32] M.E. Gurtin, D. Polignone, and J. Vinals. Two–phase binary fluids and immiscible fluids described by an order parameter. *Mathematical Models and Methods in Applied Sciences*, 6(6):815–831, 1996.

[33] H.S. Hele-Shaw. The flow of water. *Nature (London)*, 58(34), 1898.

[34] C.W. Hirt and B.D. Nichols. Volume of fluid (vof) method for the dynamics of free boundaries. *Journal of Computational Physics*, 39(1):201–225, 1981.

[35] T.J.R. Hughes, J.A. Cottrell, and Y. Bazilevs. Isogeometric analysis: CAD, finite elements, NURBS, exact geometry and mesh refinement. *Computer Methods in Applied Mechanics and Engineering*, 194(39-41):4135–4195, 2005.

[36] S. Hysing, S. Turek, D. Kuzmin, N. Parolini, E. Burman, S. Ganesan, and L. Tobiska. Quantitative benchmark computations of two–dimensional bubble dynamics. *International Journal for Numerical Methods in Fluids*, 60(11):1259–1288, 2009.

[37] D. Jacqmin. Calculation of two–phase Navier–Stokes flows using phase–field modeling. *Journal of Computational Physics*, 155(1):96–127, 1999.

[38] K.E. Jansen, C.H. Whiting, and G.M. Hulbert. A generalized–α method for integrating the filtered Navier–Stokes equations with a stabilized finite element method. *Computer Methods in Applied Mechanics and Engineering*, 190(3-4):305–319, 2000.

[39] H-G. Lee, J.S. Lowengrub, and J. Goodman. Modeling pinchoff and reconnection in a Hele–Shaw cell. I. The models and their calibration. *Physics of Fluids*, 14(2):492–513, 2002.

[40] H-G. Lee, J.S. Lowengrub, and J. Goodman. Modeling pinchoff and reconnection in a Hele–Shaw cell. II. Analysis and simulation in the nonlinear regime. *Physics of Fluids*, 14(2):514–545, 2002.

[41] J. Liu, L. Dedè, J.A. Evans, M.J. Borden, and T.J.R. Hughes. Isogeometric analysis of the advective Cahn–Hilliard equation: spinodal decomposition under shear flow. *Journal of Computational Physics*, 242:321–350, 2013.

[42] J. Lowengrub and L. Truskinovsky. Quasi–incompressible Cahn–Hilliard fluids and topological transitions. *Proceedings of the Royal Society of London, A*, 454(1978):2617–2654, 1998.

[43] J.W. McLean and P.G. Saffman. The effect of surface tension on the shape of fingers in a Hele Shaw cell. *Journal of Fluid Mechanics*, 102:455–469, 1981.

[44] S. Osher and R. Fedkiw. *Level Set Methods and Dynamic Implicit Surfaces*. Springer–Verlag, New York, 2003.

[45] R.L. Pego. Front migration in the nonlinear Cahn Hilliard equation. *Proceedings of the Royal Society of London, A*, 422(1863):261–278, 1989.

[46] L. Piegl and W. Tiller. *The NURBS Book*. Springer–Verlag, New York, 1997.

[47] F. Della Porta and M. Grasselli. On the nonlocal Cahn–Hilliard–Brinkman and Cahn–Hilliard–Hele–Shaw systems. *Communications on Pure and Applied Analysis*, 15(2):299–317, 2016.

[48] Y. Saad. *Iterative Methods for Sparse Linear Systems*. SIAM, Philadelphia, 2003.

[49] P.G. Saffman and G.I. Taylor. The penetration of a fluid into a porous medium or Hele–Shaw cell containing a more viscous liquid. *Proceedings of the Royal Society of London, A*, 45(1242):312–329, 1958.

[50] J.A. Sethian. *Level Set Methods and Fast Marching Methods*. Cambridge University Press, Cambridge, 1999.

[51] A. Tagliabue, L. Dedè, and A. Quarteroni. Isogeometric analysis and error estimates for high order partial differential equations in fluid dynamics. *Computers & Fluids*, 102(Supplement C):277 – 303, 2014.

[52] X. Wang and H. Wu. Long–time behavior for the Hele–Shaw–Cahn–Hilliard system. *Asymptotic Analysis*, 2012 (to appear).

[53] X. Wang and Z. Zhang. Well-posedness of the heleshawcahnhilliard system. *Annales de l'Institut Henri Poincare (C) Non Linear Analysis*, 30(3):367 – 384, 2013.

[54] S.M. Wise. Unconditionally stable finite difference, nonlinear multigrid simulation of the Cahn–Hilliard–Hele–Shaw system of equations. *Journal of Scientific Computing*, 44(1):38–68, 2010.

[55] O. Wodo and B. Ganapathysubramanian. Computationally efficient solution to the Cahn—Hilliard equation: adaptive implicit time schemes, mesh sensitivity analysis and the 3D isoperimetric problem. *Journal of Computational Physics*, 230(15):6037–6060, 2011.

[56] R.A. Wooding and H.J. Morel-Seytoux. Multiphase fluid flow through porous media. *Annual Review of Fluid Mechanics*, 8:233–274, 1976.

MOX Technical Reports, last issues

Dipartimento di Matematica
Politecnico di Milano, Via Bonardi 9 - 20133 Milano (Italy)

53/2017 Bertagna, L.; Deparis, S.;Formaggia, L.; Forti, D.; Veneziani A.
The LifeV library: engineering mathematics beyond the proof of concept

50/2017 Formaggia, F.; Vergara, C.
Defective boundary conditions for PDEs with applications in haemodynamics

51/2017 Gerbi, A.; Dede', L.; Quarteroni, A.
A monolithic algorithm for the simulation of cardiac electromechanics in the human left ventricle

52/2017 Beretta, E.; Ratti, L.; Verani, M.
A phase-field approach for the interface reconstruction in a nonlinear elliptic problem arising from cardiac electrophysiology

49/2017 Antonietti, P. F.,; Pennesi, G.
V-cycle multigrid algorithms for discontinuous Galerkin methods on non-nested polytopic meshes

48/2017 Regazzoni, F.; Dedè, L.; Quarteroni, A.
Active contraction of cardiac cells: a model for sarcomere dynamics with cooperative interactions

47/2017 Menghini, F.; Dede, L.; Forti, D.; Quarteroni, A.
Hemodynamics in a left atrium based on a Variational Multiscale-LES numerical model

46/2017 Agosti, A.; Gower, A.L.; Ciarletta, P.
The constitutive relations of initially stressed incompressible Mooney-Rivlin materials

45/2017 Gasperoni, F.; Ieva, F.; Paganoni, A.M.; Jackson C.H.; Sharples L.D.
Nonparametric frailty Cox models for hierarchical time-to-event data

44/2017 Martino, A.; Ghiglietti, A.; Ieva, F.; Paganoni, A.M.
A k-means procedure based on a Mahalanobis type distance for clustering multivariate functional data